Mineralium Deposita (2006) 40: 769–801
DOI 10.1007/s00126-005-0009-7

ARTICLE

Geordie Mark · Nicholas H. S. Oliver
Patrick J. Williams

Mineralogical and chemical evolution of the Ernest Henry Fe oxide–Cu–Au ore system, Cloncurry district, northwest Queensland, Australia

Received: 14 September 2004 / Accepted: 7 July 2005 / Published online: 1 February 2006

Abstract The Ernest Henry Cu–Au deposit was formed within a zoned, post-peak metamorphic hydrothermal system that overprinted metamorphosed dacite, andesite and diorite (ca 1740–1660 Ma). The Ernest Henry hydrothermal system was formed by two cycles of sodic and potassic alteration where biotite–magnetite alteration produced in the first cycle formed ca 1514 ± 24 Ma, whereas paragenetically later Na–Ca veining formed ca 1529 $+11/-8$ Ma. These new U–$Pb_{titanite}$ age dates support textural evidence for incursion of hydrothermal fluids after the metamorphic peak, and overlap with earlier estimates for the timing of Cu–Au mineralization (ca 1540–1500 Ma). A distal to proximal potassic alteration zone correlates with a large (up to 1.5 km) K–Fe–Mn–Ba enriched alteration zone that overprints earlier sodic alteration. Mass balance analysis indicates that K–Fe–Mn–Ba alteration—largely produced during pre-ore biotite- and magnetite-rich alteration—is associated with K–Rb–Cl–Ba–Fe–Mn and As enrichment and Na, Ca and Sr depletion. The aforementioned chemical exchange almost precisely counterbalances the mass changes associated with regional Na–Ca alteration. This initial transition from sodic to potassic alteration may have been formed during the evolution of a single fluid that evolved via alkali exchange during progressive fluid-rock interaction. Cu–Au ore, dominated by co-precipitated magnetite, minor specular hematite, and chalcopyrite as breccia matrix, forms a pipe-like body at the core of a proximal alteration zone dominated by K-feldspar alteration. Both the core and K-feldspar alteration overprint Na–Ca alteration and biotite–magnetite (K–Fe) alteration. Ore was associated with the concentration of a diverse range of elements (e.g. Cu, Au, Fe, Mo, U, Sb, W, Sn, Bi, Ag, F, REE, K, S, As, Co, Ba and Ca). Mineralization also involved the deposition of significant barite, K(–Ba)–feldspar, calcite, fluorite and complexly zoned pyrite. The complexly zoned pyrite and variable K–(Ba)–feldspar versus barite associations are interpreted to indicate fluctuating sulphur and/or barium supply. Together with the alteration zonation geochemistry and overprinting criteria, these data are interpreted to indicate that Cu–Au mineralization occurred as a result of fluid mixing during dilation and brecciation, in the location of the most intense initial potassic alteration. A link between early alteration (Na–Ca and K–Fe) and the later K-feldspathization and the Cu–Au ore is possible. However, the ore-related enrichments in particular elements (especially Ba, Mn, As, Mo, Ag, U, Sb and Bi) are so extreme compared with earlier alteration that another fluid, possibly magmatic in origin, contributed the diverse element suite geochemically independently of the earlier stages. Structural focussing of successive stages produced the distinctive alteration zoning, providing a basis both for exploration for similar deposits, and for an understanding of ore genesis.

Keywords Proterozoic · Hydrothermal fluids · Alteration zoning · Sodic · Potassic · Exploration vectors

Editorial handling: R. Moritz

G. Mark · N. H. S. Oliver · P. J. Williams
Economic Geology Research Unit School of Earth Sciences, James Cook University, Townsville, Qld 4811, Australia

G. Mark (✉)
Monash Ore Geology Research and Exploration Group School of Geosciences, Monash University, Clayton, PO Box 28E, Victoria 3800, Australia
E-mail: geordie.Mark@sci.monash.edu.au
Tel.: +61-3-99055764
Fax: +61-3-99054903

Introduction

Ernest Henry (Fig. 1) is the largest of a diverse group of Fe oxide–Cu–Au deposits in the Cloncurry district (Williams 1998; Williams and Pollard 2003). With a resource of 167 Mt @ 1.1% Cu and 0.54 ppm Au (Ryan 1998), Ernest Henry is Australia's second largest (after Olympic Dam) Fe oxide–(Cu–Au) deposit. Fe oxide–Cu–Au deposits are hosted mostly in Precambrian

rocks (e.g. Gawler Craton and Cloncurry district, Australia; Norrbotten, Sweden; Wernecke Mountains and Great Bear Batholith, Canada; and Carajàs, Brazil), although economically significant deposits also formed in continental margin arc settings during the Mesozoic (e.g. Candelaria-Punta del Cobre and Manto Verde, Chile). They show substantial variations in chemical and mineralogical associations, depositional ages, structural controls, and oxide and sulphide relationships in time and space (Davidson 1998; Rotherham et al. 1998; Mark et al. 2000; Skirrow 2000; Williams and Skirrow 2000; Baker et al. 2001; Skirrow and Walshe 2002). Many Fe oxide–Cu–Au terranes contain both Kiruna-type Fe oxide–apatite ironstones, where paragenetic and geochronological constraints suggest that the ironstones typically predate Cu–Au mineralization (cf. Hitzman 2000; Edfeldt and Martinsson 2003). The inter-relationships of these deposit types are relatively poorly understood, and are only now being studied in detail (Mathur et al. 2002; Edfelt and Martinsson 2003).

Furthermore, the relationships of Fe oxide Cu–Au deposits to regional hydrothermal systems are a long-standing controversy. The main points of contention concern the role(s) of coeval intrusions, metamorphic country rocks and basinal/meteoric fluids, and the sources of metals, sulphur and ligands in the ore-forming fluids (Oreskes and Einaudi 1992; Williams 1994; Haynes et al. 1995; Barton and Johnson 1996; Rotherham et al. 1998; Hitzman 2000; Mark et al. 2000; Pollard 2000; Williams et al. 2001; Mathur et al. 2002; Skirrow and Walshe 2002; Oliver et al. 2004). This controversy is in part due to the differences in the scales of regional alteration and Cu–Au mineralization, and also the complementary relationship between the suite of elements depleted during early regional alteration, but later enriched during ore deposition (e.g. K, Fe, Rb, Cu and Ba) (cf. Dilles et al. 1995; Barton and Johnson 1996). Unfortunately, there are few well-exposed or documented examples that preserve both the large-scale processes of regional alteration, and the finer scale details of

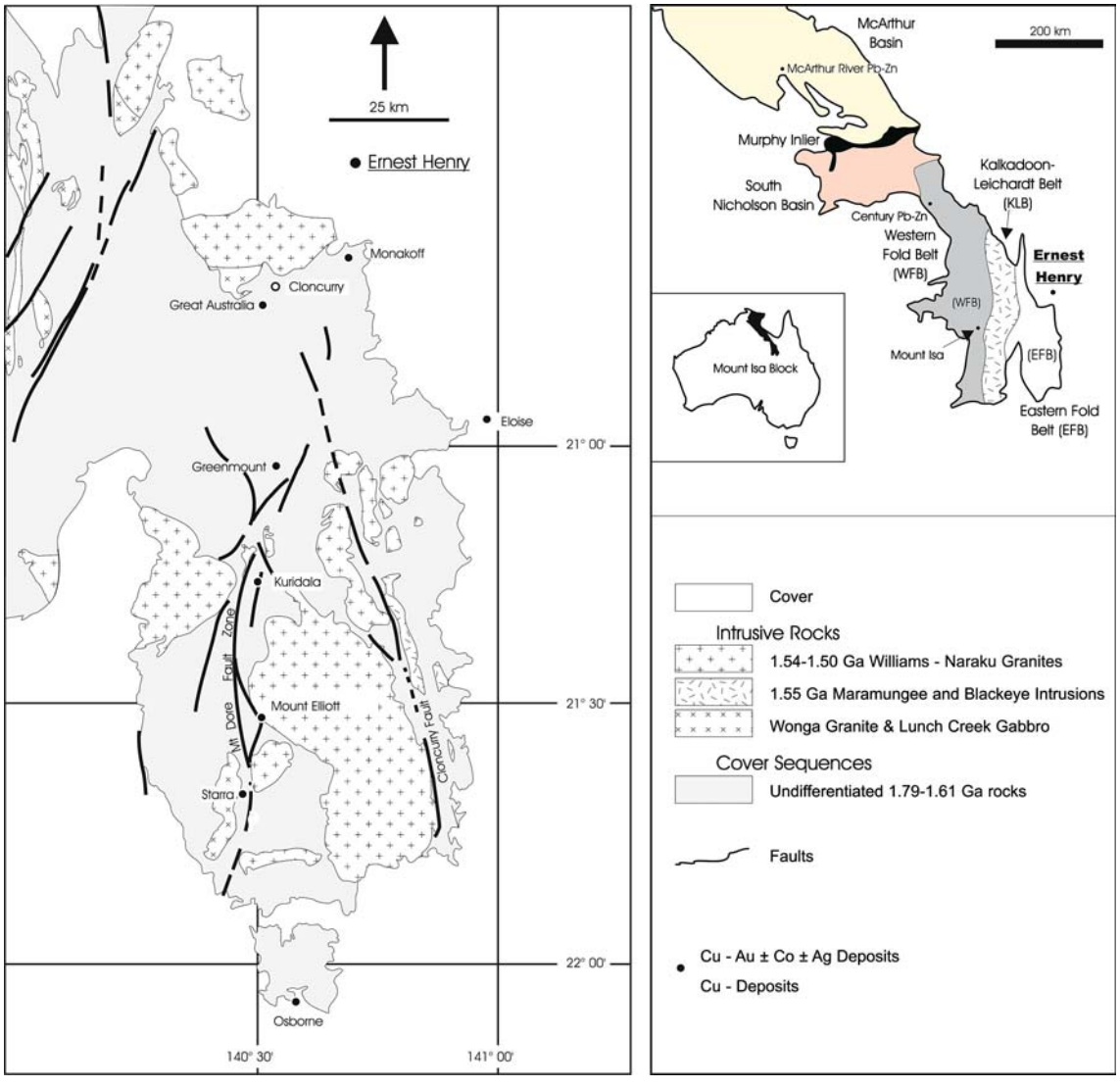

Fig. 1 The geology and mineral deposits of the Cloncurry district compiled from published AGSO maps and modified by Williams (1998)

Cu–Au hydrothermal mineralization. In the Cloncurry District, for example, all significant deposits discovered since the early 1990s occur beneath Mesozoic, Tertiary and more recent cover, and their positive magnetic signatures were initially detected by airborne magnetic surveys. As such the completion of a 42 km^2 exploration drilling program around the otherwise 'blind' Ernest Henry deposit provides an unique opportunity to study the space, time and geochemical relationships between deposit-localized potassic alteration and Cu–Au mineralization, and regional-style Na–Ca alteration.

The aim of this paper is to provide a detailed description of the temporal, spatial and geochemical evolution of the Ernest Henry hydrothermal system that adds to previous studies of Blake et al. (1997), Twyerould (1997) and Mark et al. (2000). This work is based on the detailed study of 120 diamond drill holes in a 16 km^2 area around the Ernest Henry mine. These holes were selected from both the mine lease—the area immediately over the ore deposit, and the surrounding term lease—the exploration lease enveloping the mine lease (cf. Fig. 2a). These results provide clear mineral-

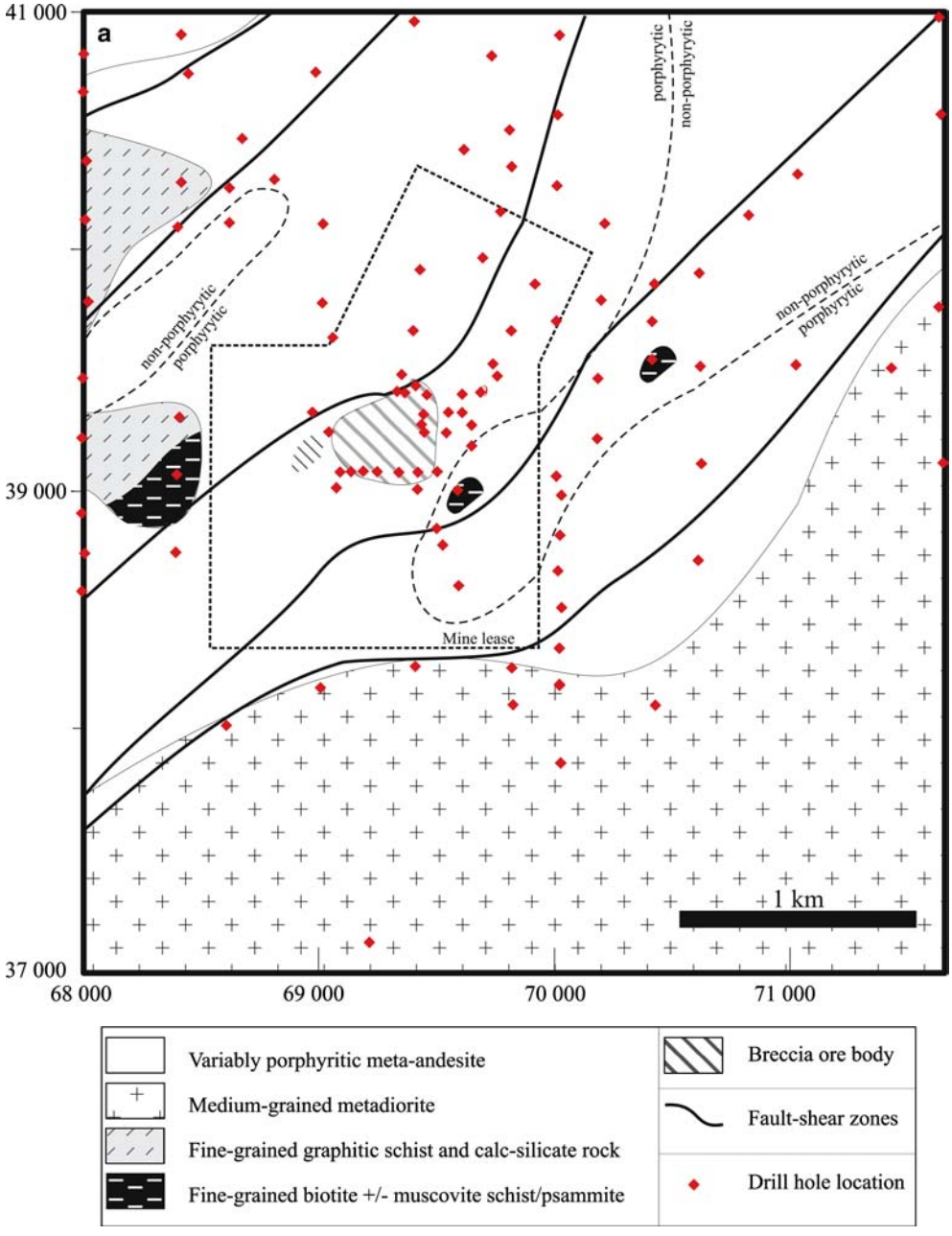

Fig. 2a Geological plan sections (at 1947 m RL, ca 200 m below current level of exposure) over the Ernest Henry orebody showing the spatial relations between rock types and alteration. **a** Geology showing the distribution of diamond drill holes logged for this study. Note that geological and geochemical data from other drill holes were included to generate this interpretation

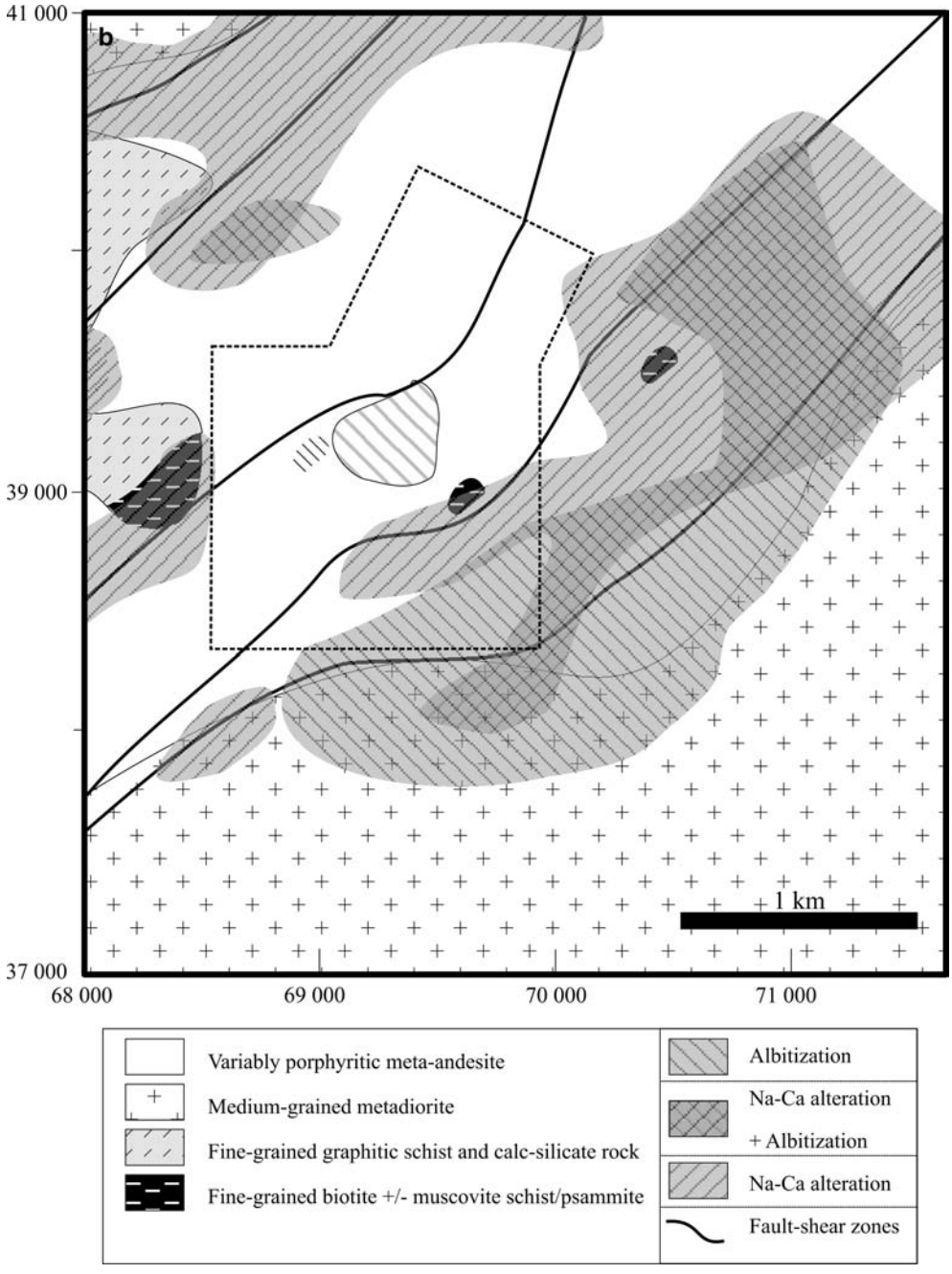

Fig. 2b Spatial relations and distribution of albitization and Na–Ca alteration

ogical and geochemical vectors towards the Cu–Au orebody applicable to explorationists employing remote and land-based geophysical and geochemical tools, and also provide a foundation for more detailed studies pertaining to ore genesis.

Regional setting

The Cloncurry district forms the easternmost exposed margin of the Mount Isa Inlier and contains many Fe oxide–(Cu–Au) deposits situated in Paleoproterozoic metasedimentary and meta-igneous rocks. Two of the three sedimentary cover sequences defined by Blake (1987) for the Mount Isa Inlier crop out in the Cloncurry district, namely, ca 1.76–1.72 Ga (cover sequence two) rocks (e.g. Page 1983; Pearson et al. 1992), dominantly composed of calcareous sedimentary rocks and various intrusive and extrusive mafic and felsic igneous rocks; and the younger ca 1.67–1.61 Ga siliciclastic sedimentary rocks of cover sequence three (cf. Blake 1987; Page and Sun 1998; Page 1998).

Polyphase deformation of the Isan Orogenies (1.60–1.50 Ga, Page and Sun 1998; Rubenach et al. 2001;

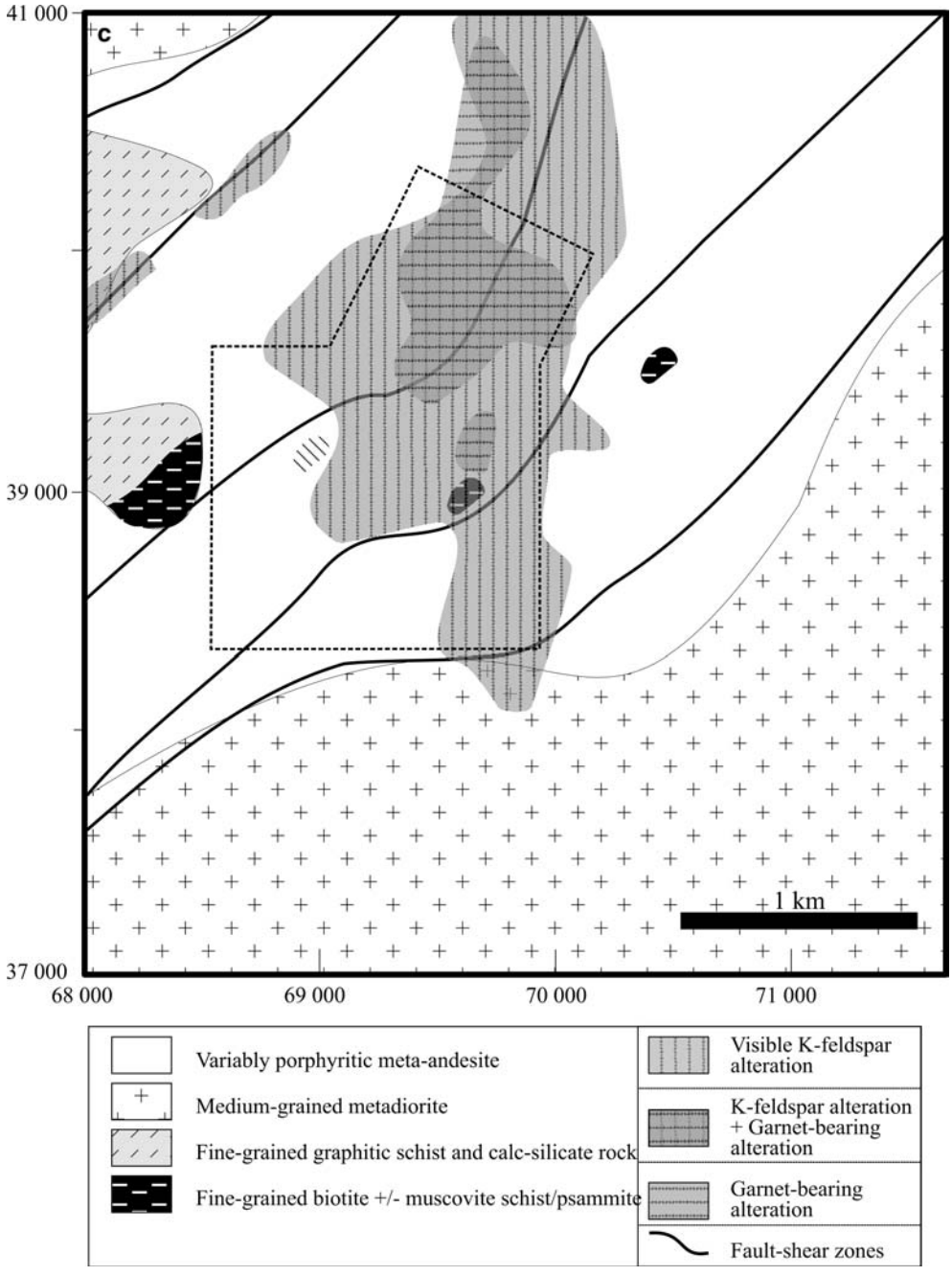

Fig. 2c Spatial relations and distribution of K-feldspathization and garnet-bearing alteration

Giles and Nutman 2002) affected these rocks, culminating in widespread igneous intrusion and mineralization (see below). The timing of metamorphism on a regional scale is poorly constrained, although recently established local geochronological constraints indicate the presence of at least two thermal peaks at ca 1.60 Ga and ca 1.55 Ga, which range in metamorphic grade from greenschist to upper amphibolite facies (Page and Sun 1998; Rubenach et al. 2001; Giles and Nutman 2002; Rubenach and Lewthwaite 2002; Oliver et al. 2004). Multiple generations of syn- and post-peak metamorphic tectonic fabrics have been recorded at many locations throughout the district (e.g. Davis et al. 2001). However, few absolute timing relations have been determined across the district, which has inhibited clear interpretations of the timing of Cu–Au ore deposits, which are all structurally controlled (Williams and Pollard 2003, and references therein; Marshall 2003).

Intrusions of the Williams and Naraku Batholiths (ca 1.55–1.50 Ga: Page et al. 1998) are volumetrically dominated by variably deformed, mafic to felsic, alkaline to subalkaline potassic phases that are predominantly metaluminous and magnetite-bearing, while contemporaneous sodic intrusive phases are rare. The

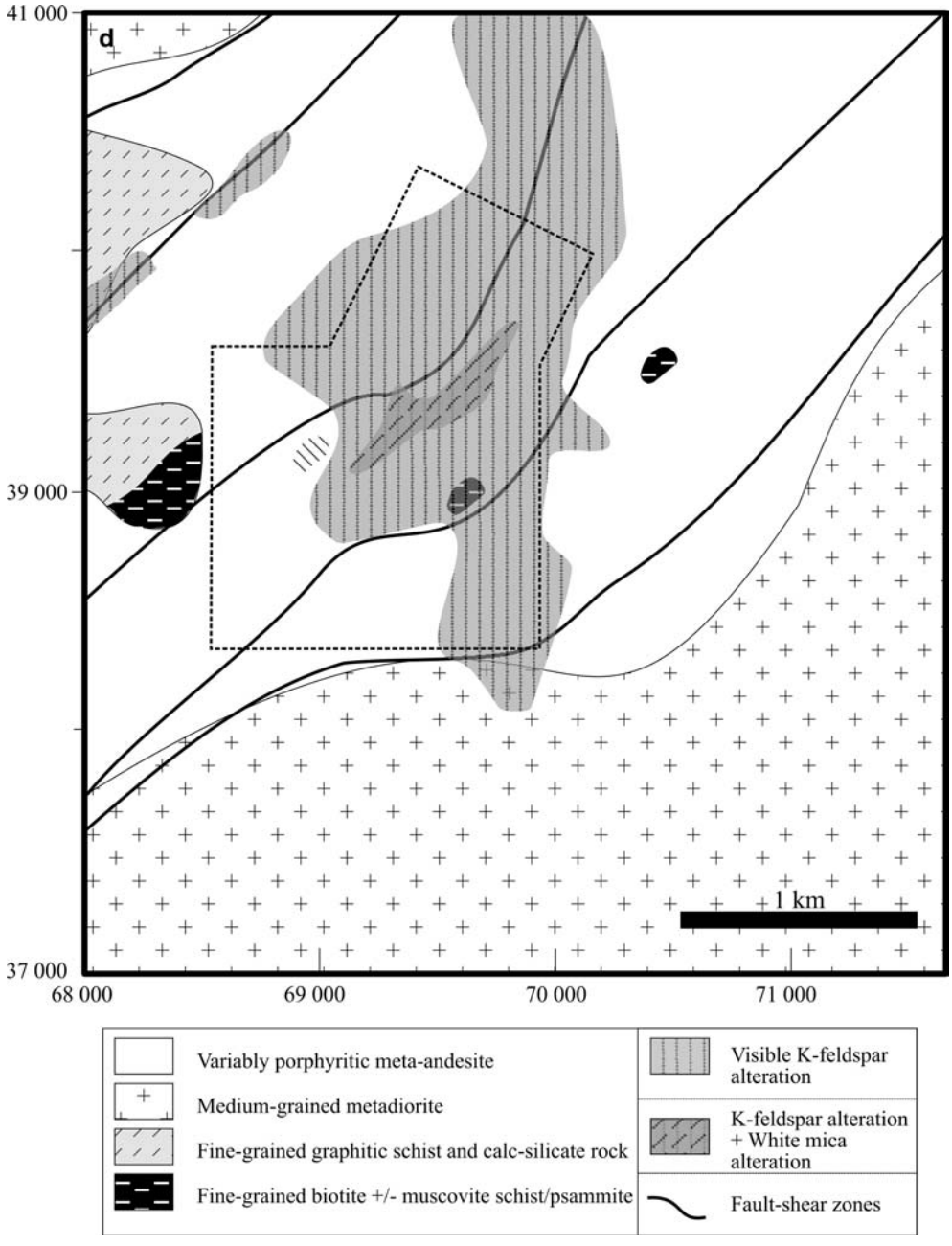

Fig. 2d Spatial relations and distribution of K-feldspathization and white mica alteration

occurrence of intra-ore intermediate dykes at the Mount Elliott Cu–Au deposit (Wang and Williams 2001), pre- to syn-ore pegmatites at the Osborne Cu–Au deposit (Gauthier et al. 2001), and complex magmatic-hydrothermal magnetite-rich mineralization within the Squirrel Hills Granite (Perring et al. 2000) provide examples of close spatial relationships between Fe oxide–(Cu–Au) mineralization and intrusions.

The district has been affected by regionally extensive (several 100 km^2) Na and Na–Ca alteration, which occurred prior to and synchronously with the intrusion of the Williams and Naraku Batholiths (ca 1.60–1.50 Ga: de Jong and Williams 1995; Pollard et al. 1998; Rubenach and Lewthwaite 2002; Mark et al. 2004a; Oliver et al. 2004). This style of alteration produced albitic plagioclase- and actinolite/tremolite-rich mineral assemblages that affected all rock types. Albite alteration also affected the host rocks within the economic Fe oxide–(Cu–Au) deposits, and typically occurred prior to Cu–Au mineralization (Adshead 1995; Baker 1996; Mark 1998; Rotherham et al. 1998). Age constraints for regional alteration and Cu–Au mineralization show that the incursion of hydrothermal fluids occurred mostly over a period of 100 million years, up to 200 million years after the formation of their host rocks (Page and Sun 1998; Perkins and Wyborn 1998; Perring et al. 2001; Gauthier et al. 2001).

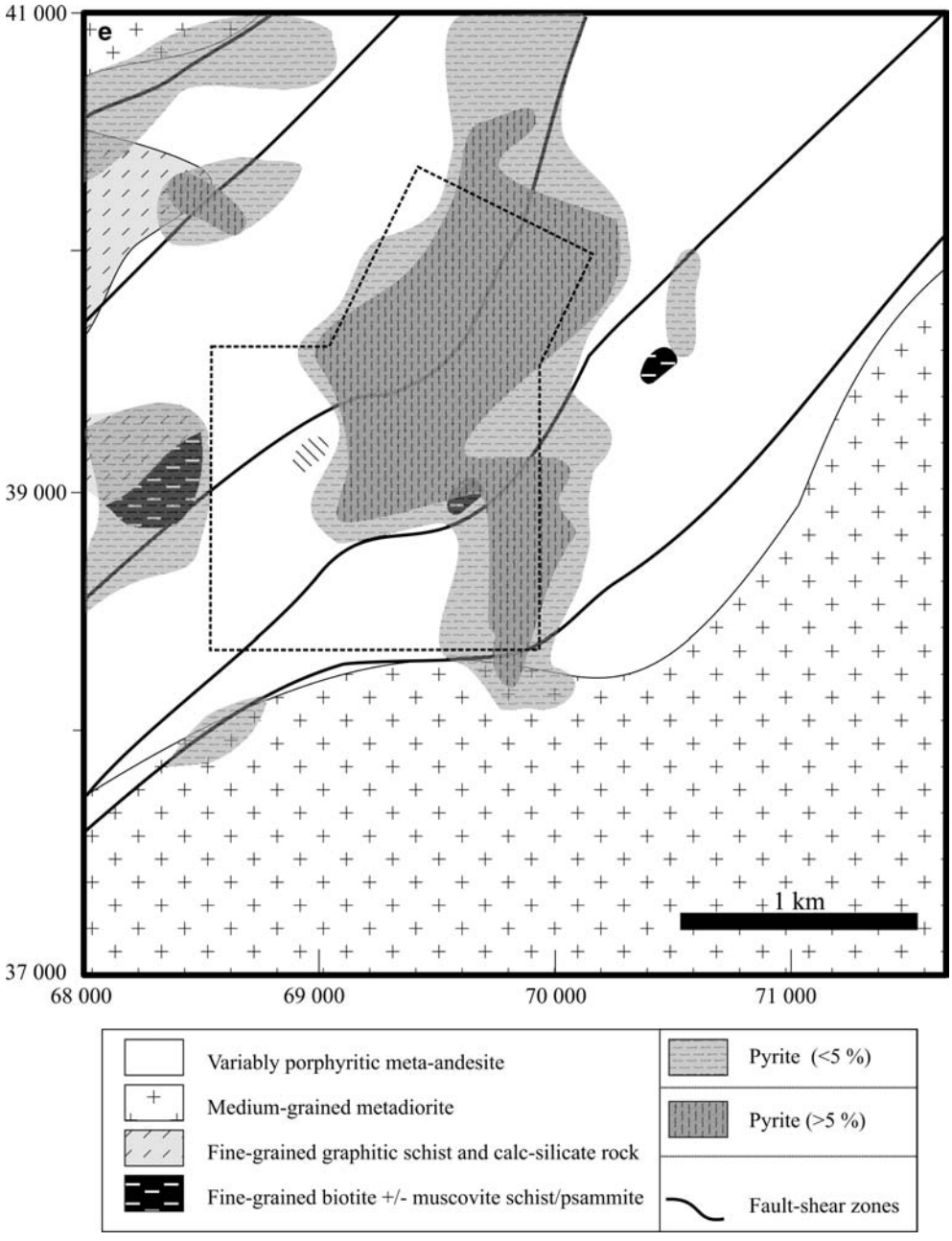

Fig. 2e Distribution of pyrite

The majority of these ore systems apparently formed synchronously with the emplacement of 1.55 to 1.50 Ga Williams-Naraku Batholith granitoid intrusions, but locally mineralization occurred somewhat earlier at ca 1.59 Ga: Gauthier et al. 2001), and possibly some developed much later (ca 340 Ma: Mark et al. 2004b).

Local geology

Host rocks

The host sequence in the Ernest Henry area (Fig. 2) is composed predominantly of plagioclase-phyric meta-andesitic rocks (Fig. 3a–e) locally intercalated with metasedimentary rocks (Fig. 3g–n) and cut by two medium-grained metadiorite intrusions (Fig. 3f) (*ca.* 1.66 Ga; Pollard and McNaughton 1997). These rocks were variably deformed and metamorphosed at lower- to middle amphibolite facies. Subsequently, they were affected by a hydrothermal alteration system and Cu–Au mineralization (cf. Fig. 2) that was largely localized around veins and breccias associated with brittle-ductile deformation along NE-trending fault zones. The emplacement environment of the meta-andesites is unclear due to the lack of preserved extrusive-related textures (e.g. flow top breccias), although these features, if

originally present, may have been destroyed by tectono-metamorphic or hydrothermal processes. The majority of these meta-andesitic rocks have a fine-grained groundmass with subhedral to euhedral plagioclase phenocrysts, and they preserve a variety of glomero-porphyritic, porphyritic, seriate to non-porphyritic igneous textures (cf. Fig. 3a–e). They are the likely temporal equivalents to similarly textured meta-igneous rocks that form the bulk of the Mount Fort Constantine rock outcrops (*ca*. 1.74 Ga; Page and Sun 1998), 10 km southwest of the deposit. The groundmass in equivalent rocks at Ernest Henry commonly has a trachytic texture (cf. Fig. 3b), and is mainly composed of plagioclase (70–85%), biotite (5–20%), magnetite (2–5%), quartz ($< 5\%$) and accessory apatite. Distinguishable individual meta-andesite units have apparent thicknesses between 1 and 60 m. Aphanitic units are mostly < 10 m thick, and volumetrically less significant. Boundaries between units can be sharp (1–3 cm) to gradual (1–2 m). Amygdale-rich horizons (containing up to 20%, over 5 m) occur in some plagioclase-phyric meta-andesites, although they are more prevalent in aphanitic variants (cf. Fig. 3c–e).

Various metasedimentary rocks (5–50 m thick) are intercalated with the meta-andesite, and comprise biotite- and muscovite-rich schist, biotite psammite, graphitic (andalusite) schist, banded scapolitic calc-silicate rock and cordierite-muscovite schist (cf. Fig. 3g–n). The most common rock types include biotite- and muscovite-rich psammite, and graphitic schist. These siliciclastic and calc-silicate metasedimentary rocks constitute only a minor component of the protoliths to the ore breccia (cf. Fig. 3g, j and m).

The two metadioritic intrusions are similar in age to batholithic plutons emplaced near Mount Isa (Sybella Granite, Wyborn et al. 1988). They are also similar in age to the cover sequence three rock packages that host the Mount Isa Cu–Pb–Zn and Cannington Ag–Pb–Zn deposits (e.g. Mount Isa Group; Page and Sweet 1998; Soldiers Cap Group, Page and Sun 1998), equivalents of which are exposed 30 km south of Ernest Henry. These intrusions are medium- (1–3 mm) to coarse-grained (5–10 mm), mesocratic to leucocratic, and equigranular, and contain plagioclase, hornblende, magnetite, titanite, quartz and K-feldspar (cf. Fig. 3f). Local mineralogical variations are presumably due to internal magmatic evolution and melt differentiation.

Deformation and metamorphism

The structural and geophysical grain of the region trends north, but bends to the NE in the vicinity of the deposit. The main shear zone foliations and faults at the mine dip moderately SE, and the breccia-hosted orebody plunges down-dip within these fabrics (Webb and Rowston 1995; Twyeroud 1997). Although the formation age of the controlling structures is poorly constrained, all individual faults and shear zones in the vicinity of the deposit exhibit evidence for episodic post-peak metamorphic hydrothermal alteration, although some were initiated prior to Cu–Au mineralization.

Three distinct ductile tectonic fabrics have been identified around Ernest Henry. However, the lack of continuity of fabric intensity along and between oriented drill core inhibits precise 3-D reconstruction of geometry and the geometric evolution. The earliest S1 fabric is preserved only in micaceous and porphyroblastic metasedimentary rocks, and occurs as a bedding-subparallel feature found outside the main ore zone. S1 is locally preserved as a closely spaced schistosity in muscovite-rich (Fig. 3i) and graphitic schist, and less commonly occurs as aligned inclusion trails within cordierite and garnet porphyroblasts, and as remnants within differentiated S2 crenulation cleavage in mica schists (cf. Fig. 3i, l). The dominant tectonic fabric distal to the ore deposit, S2, appears to have formed broadly synchronous with the growth of peak amphibolite facies metamorphic minerals (Fig. 3i–j). D2 commonly produced 5–10 mm crenulations of S1, 1–10 cm open folds, and most commonly, a closely-spaced penetrative tectonic fabric (S2), especially in the vicinity of the ore deposit and within its bounding shear zones (cf. Fig. 3i–n). S2 fabrics outside the mine lease are locally overprinted by albite veining and porphyroblastic albite formed during the earliest stages of the Ernest Henry hydrothermal system (Fig. 3l–n, see below). The youngest ductile tectonic fabrics (S3) are most intense within the mine lease, and are commonly identified by a heterogeneous foliation (S3) and local crenulation development and formation of imbricate breccias in biotite and/or carbonate-rich horizons within and directly adjacent to the ore breccia. S3 fabrics locally overprint products of biotite–magnetite alteration in the footwall and hanging wall rocks, and are rarely observed to have folded K-feldspar–quartz–rutile veins produced immediately prior to Cu–Au mineralization (see below).

Hydrothermal alteration distribution and paragenesis

The Ernest Henry hydrothermal evolution (Table 1, Fig. 4) is broadly divisible into chemical and mineralogical associations representing products of early Na and Na–Ca alteration, pre-ore K–(Mn–Ba)-rich alteration and Cu–Au mineralization. The hydrothermal alteration around the deposit is largely controlled by NE-trending faults, fault zones adjacent to metadiorite intrusions, and along the extensions of the fault/shear zones that bound the orebody (Fig. 2a–b). For the most part, hydrothermal alteration associated with Na and Na–Ca alteration is largely preserved in vein, breccia and replacement features focused in the NE-trending fault zones distal to the deposit, whereas younger K-feldspar and biotite veining predominate around the ore breccia and transgress the NE-trending fault arrays. Cu–Au mineralization and hydrothermal brecciation occurred within the potassically altered rocks between shear zones bounding the orebody.

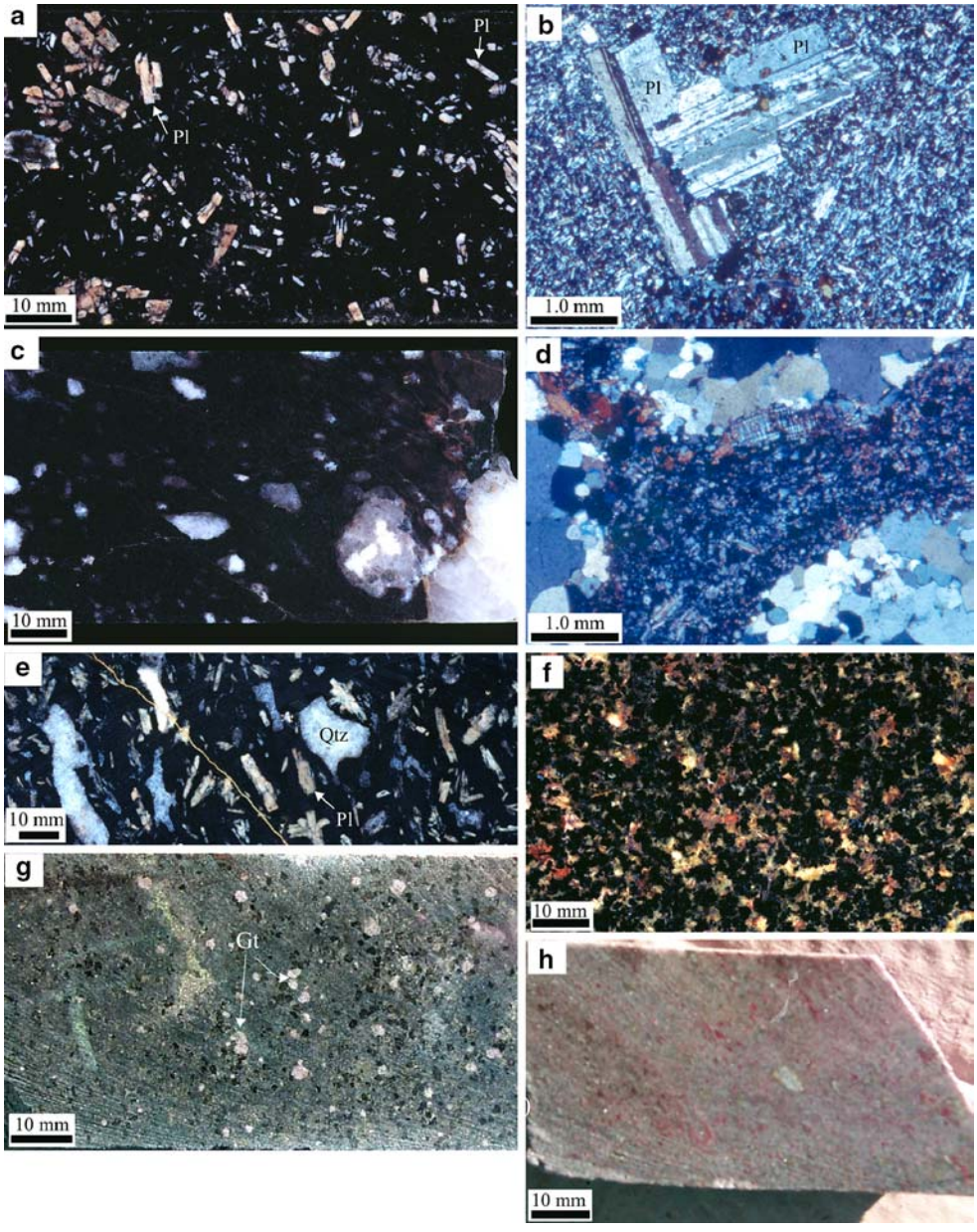

Fig. 3 Pictures of the main rock types (e.g. meta-andesite, meta-diorite, and siliciclastic and calc-silicate rocks) around Ernest Henry. Mineral abbreviations after Kretz (1983); Ab, albite; And, andalusite; Bt, biotite; Gt, garnet; Po, pyrrhotite; Qtz, quartz; Scp, scapolite; XP, cross polarized light; PP, plain polarized light. **a** Seriate textured plagioclase phyric meta-andesite with a fine-grained, biotite-rich matrix (FTCD 2047, 236.0 m). **b** Porphyritic meta-andesite (XP) with a fine-grained intergranular plagioclase-rich matrix (FTCD 2047, 236.0 m). **c** Amygdale-bearing meta-andesite with a fine-grained, biotite-rich matrix. The amygdales are composed of quartz and calcite (FTCD 2179, 237.6 m). **d** Amygdaloidal meta-andesite (XP) with a fine-grained feldspathic groundmass locally affected by hematitic K-feldspar alteration (FTCD 2040, 244.0 m). **e** Quartz amygdale-bearing plagioclase phyric meta-andesite with a fine-grained biotite-rich matrix (FTCD 2147, 245.0 m). **f** Medium-grained, equigranular metadiorite composed of hornblende, plagioclase, magnetite and quartz (FTCD 2022, 250.1 m). **g** Medium-grained scapolitic calc-silicate rock that was altered by porphyroblastic garnet during Cu–Au mineralization (FTCD 32, 409.9 m). **h** Medium-grained, equigranular muscovite psammite representative of metasedimentary rocks intercalated with plagioclase phyric meta-andesite in the orebody (FTCD 32, 376.9 m). **i** Andalusite-biotite schist preserving both S1 and S2. Note the syn- to post-S2 timing of andalusite growth (FTCD 2175, 240.0 m). **j** Scapolite-biotite calc-silicate rock (cf. Fig. 3m). The meionitic scapolite contains aligned inclusions that define a relict S2 fabric (XP) (FTCD 2171, 264.6 m). **k** Selective pyrrhotite alteration of biotite in a fine-grained biotite psammite at the margin of a quartz-pyrrhotite vein (PP) (FTCD 2171, 246.2 m). **l** Differentiated S2 crenulation cleavage defined by aligned metamorphic muscovite later overprinted by porphyroblastic albite associated with earlier albitization (XP) (FTCD 2175, 240.2 m). **m** Meionitic scapolite-biotite calc-silicate rock overprinted (right) by light coloured albite, diopside, actinolite and pyrite alteration associated with stage 1 Na–Ca alteration (FTCD 2076, 226.0 m). **n** Muscovite-biotite schist preserving the local S2 tectonic fabric overprinted by fine-grained albite associated with early albitization (FTCD 2175, 230.0 m)

Fig. 3 (Contd.)

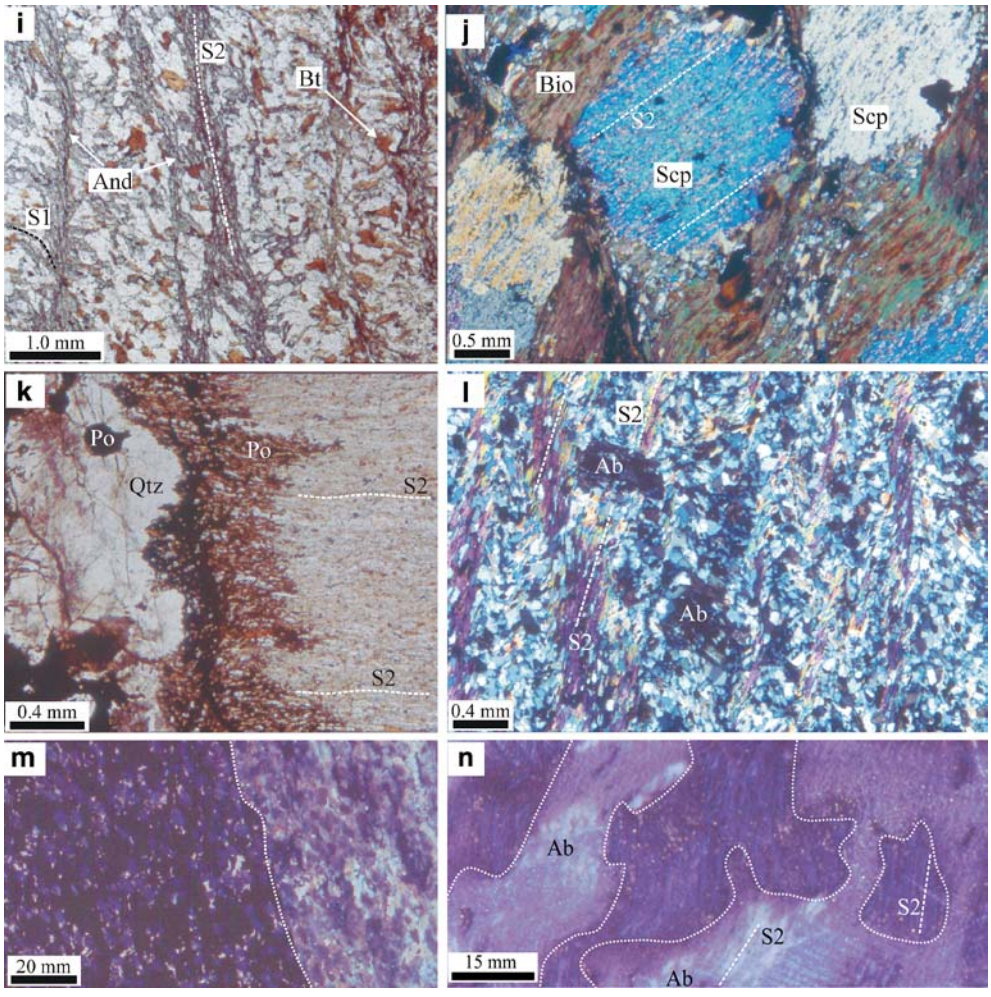

Na and Na–Ca alteration

The earliest metasomatism involved intense Na (cf. Fig. 3n, 5a–d) and Na–Ca alteration (cf. Fig. 3m, 5b, e–f), particularly albitization (Table 1, Fig. 4). These homogeneously fine-grained, albitic-altered rocks are largely preserved outside the bounds of the mine lease, occurring mainly along NE-trending contacts between metadiorite and metasedimentary rocks (Fig. 2b). This spatial association indicates that the albitizing fluids were structurally controlled along fractures, faults, and lithological contacts, as noted regionally in the Eastern Fold Belt (Oliver et al. 1990; Rubenach and Lewthwaite 2002). The antipathetic relationship between areas of Na–Ca and K–(Mn–Ba) alteration (Fig. 2b–c) is partly related to strong overprinting by the latter, which mostly obliterated previous Na and Na–Ca alteration. The albitized rocks are cut and replaced by K-feldspar and or biotite in the hanging wall, and rare relict albite grains occur within K-feldspar altered breccia clasts in the orebody (cf. Fig. 4a, b and n).

Other minerals in Na–Ca altered rocks include minor actinolite, diopside, magnetite, scapolite and pyrite (cf. Fig. 3b, e–f, and m). Relatively, albite-poor calcic alteration (containing actinolite, magnetite, diopside and pyrite) selectively affected primary ferromagnesian minerals in metadioritic rocks on the margins of the more-intensely albitized zones. Locally intense scapolitic alteration (Me_{20-40}) is common and is associated with diopside, actinolite, quartz and pyrite veining. Clast- and matrix-supported breccias are common, and resemble those linked to regional Na–Ca alteration elsewhere in the Cloncurry district (de Jong and Williams 1995; Marshall 2003). Fine- to coarse-grained magnetite, apatite, actinolite, quartz and pyrite vein associations are rare, and form 10- to 100-m scale weakly Cu-enriched bodies in the footwall and hanging wall to the deposit (Fig. 5g).

Pre-ore K–(Mn–Ba)-rich alteration

Dark-coloured, fine-grained biotite- and magnetite-rich alteration (with rare K-feldspar) overprinted albitized rocks, and formed a significant alteration halo best developed in the plagioclase-phyric meta-igneous rocks, although the original intensity of this alteration is obscured in, and immediately around, the orebody.

The alteration intensity is variable, being greatest in relatively ferromagnesian-rich rocks. This alteration type occurs relatively early in the hydrothermal paragenesis and is commonly overprinted by Na–Ca veining and K-feldspar alteration associated with Cu–Au mineralization. However, as opposed to the aforementioned fine-grained alteration, later garnet-, K-feldspar- and biotite-rich alteration assemblages were largely localized in the northeast portion of the mine lease and affected footwall rocks for more than 1 km away from the orebody (Figs. 2c and 5i). Garnet in these assemblages is Mn-rich, locally contains up to 49 mole percent spessartine (Tables 2, 3, 4), occurs as both infill and hydrothermal replacement, and is typically coarse-grained. The K-feldspar is typically Ba-enriched (up to 3 wt% BaO, Tables 2, 3, 4), although individual grains exhibit significant compositional variation (cf. Fig. 5m).

Ore-stage associations

In plan section, the extent of potassically altered rock extends to >1 km beyond the mine (cf. Fig. 2 a–b), but it is most intense in the vicinity of the orebody (cf. Fig. 5a,b and h). Potassically altered rocks also occur along the main NE-trending fault zones, and locally overprints Na–Ca alteration, biotite–magnetite alteration and magnetite-apatite-rich veining (cf. Fig. 5a,b and h). This association comprises veins, breccia and hydrothermal replacement that are K-feldspar dominant. Veins bearing K-feldspar, quartz, rutile and calcite are commonly parallel to, boudinaged by, and cut the local S3 tectonic fabric. K-feldspar alteration preferentially affected plagioclase phyric meta-andesite horizons. Minor fine-grained muscovite alteration is apparent and occurs peripheral to the high-grade parts of the orebody.

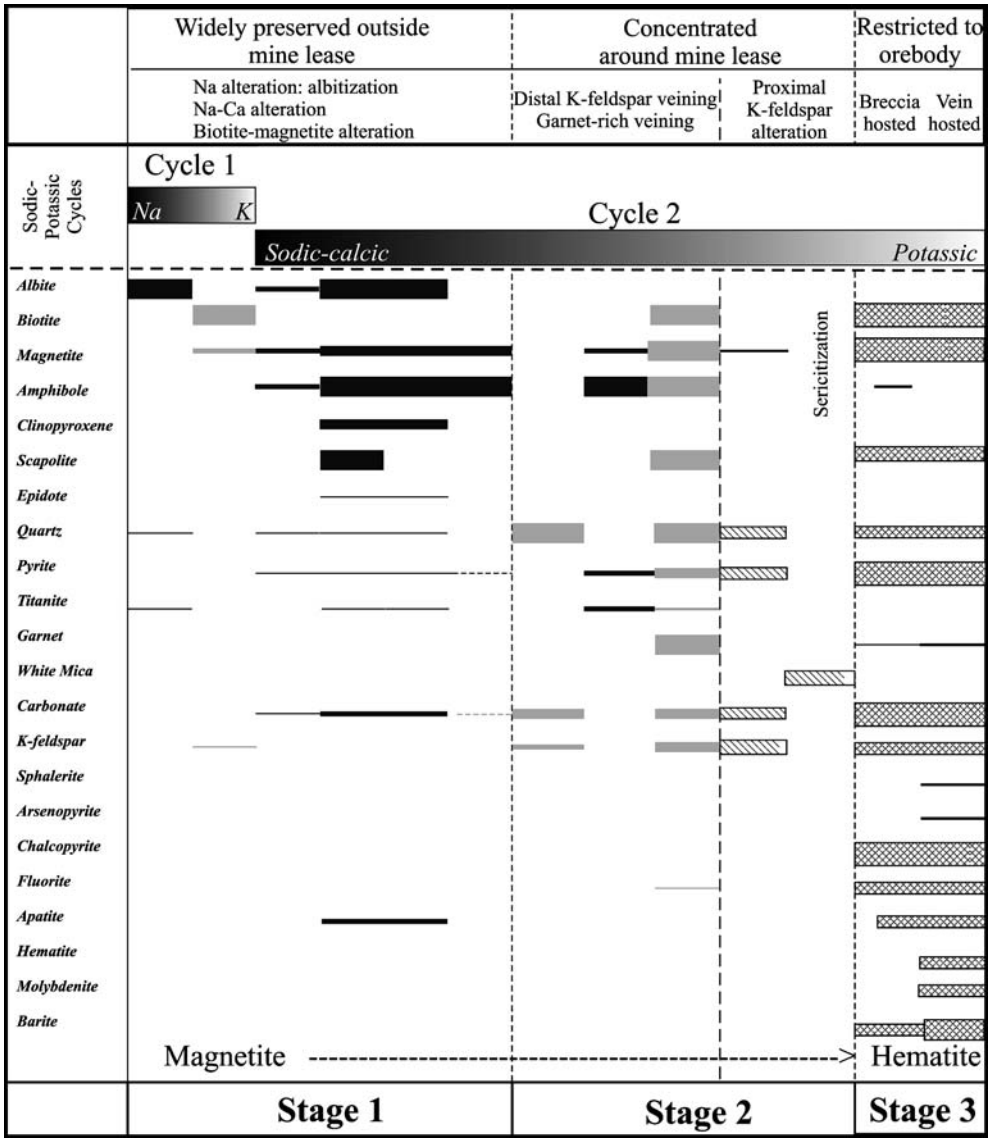

Fig. 4 Paragenetic sequence and spatial distribution of pre- and syn-ore hydrothermal alteration in the Ernest Henry term lease. The sequence is divided into three main phases: 1) Stage 1, which largely refers to hydrothermal associations produced during the earlier stages of hydrothermal evolution (e.g. albitization and Na–Ca alteration); 2) Stage 2, which refers to hydrothermal associations chemically-linked, but occurring prior to Cu–Au mineralization; and, 3) Stage 3, which relates to hydrothermal associations temporally, spatially and chemically linked to the ore. The width of individual lines refers to the relative abundance of a mineral formed during a particular stage, where stippled lines represent trace mineral abundances, whereas the thickest solid line shows that a mineral is present in abundance. Bllack fill denotes relatively Na-rich pre-ore mineral assemblages, and grey fill highlights K-rich mineral assemblages deposited prior to ore-related K-feldspar alteration. Other fills ae specific to individual mineral phases

Table 1 Summary of the mineralogical characteristics, style and chemistry of the main hydrothermal associations in the Ernest Henry term lease. Data compiled from drill core, whole rock geochemistry, mineral chemistry and petrographic analysis (this study; Blake et al. 1997; Twyerould 1997)

Hydrothermal Alteration	Mineralogy (vein and alteration)	General Alteration Characteristics	Rock Types	Hydrothermal Styles	Spatial relations to Cu–Au mineralisation	Main Chemical Associations
Pre-ore Sodic alteration						
Albitization	albite, titanite, quartz	fine-grained albitization minor titanite, mainly present in altered diorite	diorite, siliciclastic metasedimentary rocks, plagioclase phyric volcanic rocks, calc-silicate rocks	pervasive fine-grained alteration, fracture-controlled breccias, veining	Present over whole area, although lack of preserved alteration in the vicinity of the orebody rare in hanging wall rocks and ore breccia clasts	Na
Na–Ca alteration	actinolite, tremolite, titanite, diopside albite, scapolite, calcite, apatite magnetite, pyrite, quartz	fine-grained albitization minor scapolite and diopside alteration minor titanite, mainly present in altered diorite	diorite, plagioclase phyric volcanic rocks, siliciclastic metasedimentary rocks, calc-silicate rocks	Fracture-related hydrothermal breccia, crackle veining, pervasive alteration	Pervasive throughout term lease, but overprinted by K-feldspar alteration in the vicinity of the ore breccia. Most intense hydrothermal breccias along NE trending fractures	Na, Ca
Magnetite-apatite	magnetite, apatite, actinolite, quartz calcite, quartz	massive fine- to coarse-grained magnetite alteration	plagioclase phyric volcanic rocks	hydrothermal veining, localized pervasive alteration	Present within NE trending fracture systems in the footwall to the deposit	Fe, P, Mg
Potassic alteration						
Biotite–magnetite	biotite, magnetite, K-(Ba) feldspar titanite, quartz	pervasive biotite alteration minor fine-grained K-feldspar with biotite	plagioclase phyric volcanic rocks, siliciclastic metasedimentary rocks	pervasive alteration, rare veining	Pervasive throughout the term lease, and affects all major rock types	K, Rb, Fe, Ba, Mn, Cl
Garnet–K-feldspar–biotite	garnet, biotite, K-feldspar, amphibole quartz, magnetite, pyrite, chalcopyrite	fine- to medium-grained biotite and garnet alteration	plagioclase phyric volcanic rocks, siliciclastic metasedimentary rocks	hydrothermal breccias, localized crackle veining, local pervasive alteration	Present largely in the footwall to the deposit, and occurs up to 1.5 kilometres from the orebody.	Fe, Mn, K, Ba, Cl, Cu, Co
Syn-ore						
K-feldspar	K-(Ba) feldspar, quartz, rutile, calcite	equigranular fine- to medium-grained K-feldspar alteration	plagioclase phyric volcanic rocks, siliciclastic metasedimentary rocks diorite, calc-silicate rocks	pervasive alteration of volcanic rocks, veining	Most intense in the vicinity of the orebody, although occurs as crackle veins up to 2 kilometres from the orebody	K, Rb, Ba, Cl, Cu, Co Ni, As
Sericite	sericite, quartz	pervasive fine- to medium-grained white mica alteration of K-feldspar altered volcanic rocks	plagioclase phyric volcanic rocks	pervasive alteration, localized crackle veining	Overprints K-feldspar altered volcanic rocks, within 400 m of the orebody	K, H

Table 1 (Contd.)

Cu–Au mineralisation						
Breccia	magnetite, pyrite, calcite, biotite, K-(Ba) feldspar,chalcopyrite, barite, molybdenite, arsenopyrite, quartz, electrum, garnet, amphibole, rutile sphalerite, galena, coffinite, monazite	equigranular K-feldspar alteration minor biotite alteration minor garnet and amphibole alteration in calc-silicate rocks minor arsenopyrite and pyrite alteration in siliciclastic metasedimentary rocks	plagioclase phyric volcanic rocks, calc-silicate rocks, siliciclastic metasedimentary rocks	infill-supported hydrothermal breccia, distal crackle veining, distal alteration	Exhibits localization from inner ore breccia to outer crackle veining Elevated Co, As and S up 150 m from ore breccia	Fe, K, Ba, S, Cu, Au, Mn, Ca, C, Sr, Co, As, Mo, Sb, U, Ag, F, Cl
Late veining	K-(Ba) feldspar, magnetite, pyrite, chalcopyrite, fluorite, molybdenite, calcite, garnet, quartz, barite, rutile	no demonstrable alteration	Stage 1 ore breccia	fracture-related veining and breccia	No demonstrable core-margin zonation within ore breccia	Fe, K, Ba, S, Cu, Au, Mn, Ca, C, Sr, Co, As, Mo, Sb, U, Ag, F, Cl

Main phase ore breccia

Ore is largely hosted by breccia that contains clasts of rounded to subrounded K-feldspar altered plagioclase phyric meta-andesite. The distributions of Cu–Au and K-feldspar altered rocks suggest the two were closely related. Breccia-hosted ore typically grades into marginal subeconomic crackle-style hydrothermal veining. The hydrothermal mineral association largely comprises magnetite, calcite, pyrite, biotite, barite, chalcopyrite, quartz, specular hematite and K-(Ba) feldspar (cf. Fig. 5j–p). Accessory minerals include molybdenite (Fig. 5o), coffinite, native gold-electrum, arsenopyrite (Fig. 5k–l), apatite, fluorite, rutile, monazite, spessartine-rich garnet, actinolite, sphalerite, scheelite and galena. Magnetite and calcite are the dominant hydrothermal matrix components (cf. Fig. 5k, m-o). The breccias are variably affected by deformation and locally contain elongate, aligned, K-feldspar altered clasts and recrystallized magnetite, calcite and sulphides in the breccia matrix. Specular hematite is uncommon. Most hematite however occurs as an alteration product after magnetite, and is mainly localized along fractures or grain boundaries. The timing and genetic relation of secondary hematite alteration to ore magnetite and ore formation is unconstrained. Biotite is enriched in both Cl and F, and is similar in composition to that in pre-ore K–(Mn–Ba)-rich alteration and post-ore veins (Tables 2, 3, 4). Apatite is also enriched in F (cf. Twyerould 1997).

Irregular veins composed of calcite, quartz, K-feldspar, magnetite, hematite, chalcopyrite, pyrite, biotite, barite, apatite and fluorite formed during ongoing dilation between the bounding shear zones (Mark et al. 2000). They overprint ore breccia and vary in thickness from 5 to >100 mm (Fig. 5p). Minor mineral phases in these veins include rutile, spessartine garnet, actinolite, molybdenite and scheelite. These veins may be regarded as the last Cu–Au mineralization stage, mostly formed after brecciation had ceased, and while ductile deformation of the surrounding shear zones was waning.

Post-ore veining and alteration

Late carbonate-rich veins and matrix-supported breccia are mainly composed of medium-grained calcite, dolomite and quartz, and fine-grained biotite, actinolite-tremolite, pyrite and magnetite (Fig. 5q). Calcite is the main mineral and is typically recrystallized to fine- and medium-grained assemblages. Biotite and magnetite alteration at the margin of veins and breccias is common, although pyrite alteration is rare. These post-ore breccias contain subrounded to rounded clasts (10–100 mm) of earlier formed ore breccia and K-feldspar altered meta-andesite. Some of the carbonates present (particularly the finer grained varieties) may represent remnants of a primary marble, as marble breccias are found regionally with similar matrix/clast relationships (Marshall 2003).

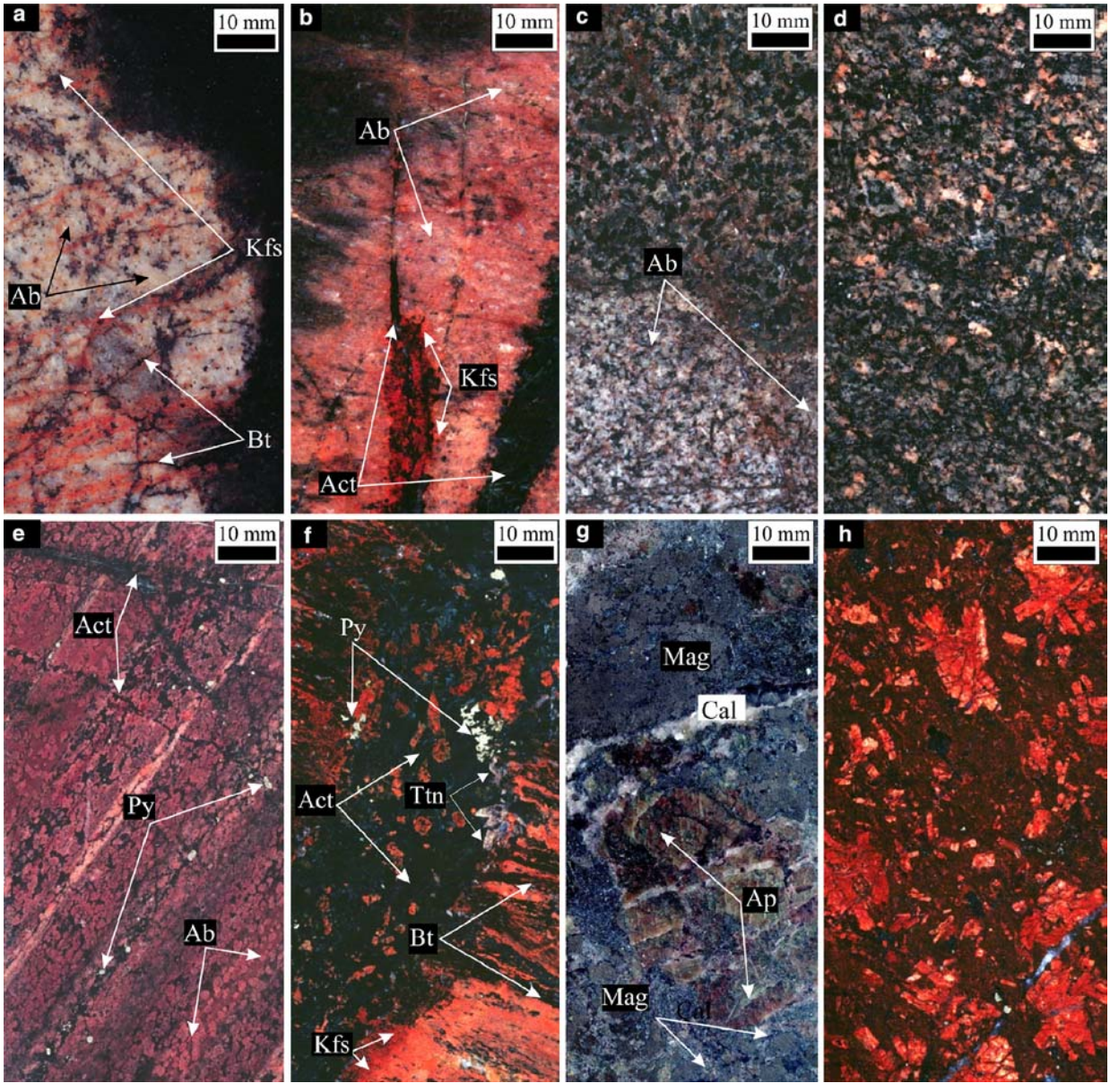

Fig. 5 Pictures showing the main styles and temporal associations of hydrothermal veins, breccias and alteration products in the term lease over Ernest Henry. Mineral abbreviations after Kretz (1983). **a** Albitized (Ab), biotite–magnetite (Bt) altered meta-andesite cut by late hematitic stained K-feldspar veins (FTCD 2157, 257.1 m). **b** Multiply altered and veined plagioclase phyric meta-andesite. Note that albitization is texturally retentive and represents the earliest phase of alteration. Actinolite veins are cut by K-feldspar- and pyrite-bearing veins (FTCD 2040, 250.35 m). **c** Irregular and sharp contact between medium-grained and albitized (Ab) metadiorite. Thin biotite-rich veins (Bt) cut zones of albitization (FTCD 2114, 241.9 m). **d** Pervasively biotite–magnetite altered equigranular medium-grained albitized metadiorite (cf. Figs. 3**d**, 4**c**) (FTCD 2163, 226.8 m). **e** Hydrothermally altered porphyroblastic scapolitic calc-silicate rock now largely composed of albitic plagioclase. The albitization processes involved the retention of the original texture. Minor actinolite overprints metamorphic biotite (FTCD 2076, 226.0 m). **f** Multiply altered fine-grained meta-andesite showing early vein-controlled biotite alteration cut by actinolite, titanite and pyrite veining. Hematitic K-feldspar cuts earlier actinolite veins (FTCD 2032, 257.0 m). **g** Coarse-grained magnetite-apatite ironstone of probable similar character to the skarn-type rocks dated by Twyerould (1997). The assemblage also contains actinolite and quartz, and is cut by late calcite veining (FTCD 48, 273.2 m). **h** K-feldspar altered glomeroporphyritic meta-andesite (FTCD 28, 443.2 m). **i** Coarse-grained Mn-rich garnet (Sps- spessartine garnet), K-(Ba) feldspar, quartz, biotite associated with pre-ore veining in plagioclase phyric meta-andesite within the footwall (FTCD 2069, 257.2 m). **j** Typical sulphide mineralized infill-supported hydrothermal ore breccia containing clasts of rounded to subrounded K-feldspar altered meta-andesite. The matrix is dominated by magnetite, pyrite, chalcopyrite and biotite (FTCD 28, 257.0 m). **k** Reflected light image of a typical example of disseminated, fine- to medium-grained magnetite (Mag)-rich ore containing chalcopyrite (Ccp) and arsenopyrite (Ars) (FTCD 28, 158.9 m). **l** Reflected light image of arsenopyrite (Ars)-bearing (locally containing inclusions of chalcopyrite), magnetite-rich ore. Note the ore matrix is largely composed of magnetite (Mag), calcite and quartz (FTCD 28, 158.9 m). **m** Back scattered electron image of a typical ore assemblage showing an irregularly zoned K-feldspar (Kfs) grain rimmed by high Ba margins. The Ba content of K-feldspar is especially high where in contact with calcite (FTCD 48, 405.5 m). **n** Back scattered electron image of a typical hydrothermal mineral association with Cu–Au mineralization. Note the presence of relict (?) albite (Ab) grain adjacent to the syn-ore K-feldspar (Kfs)

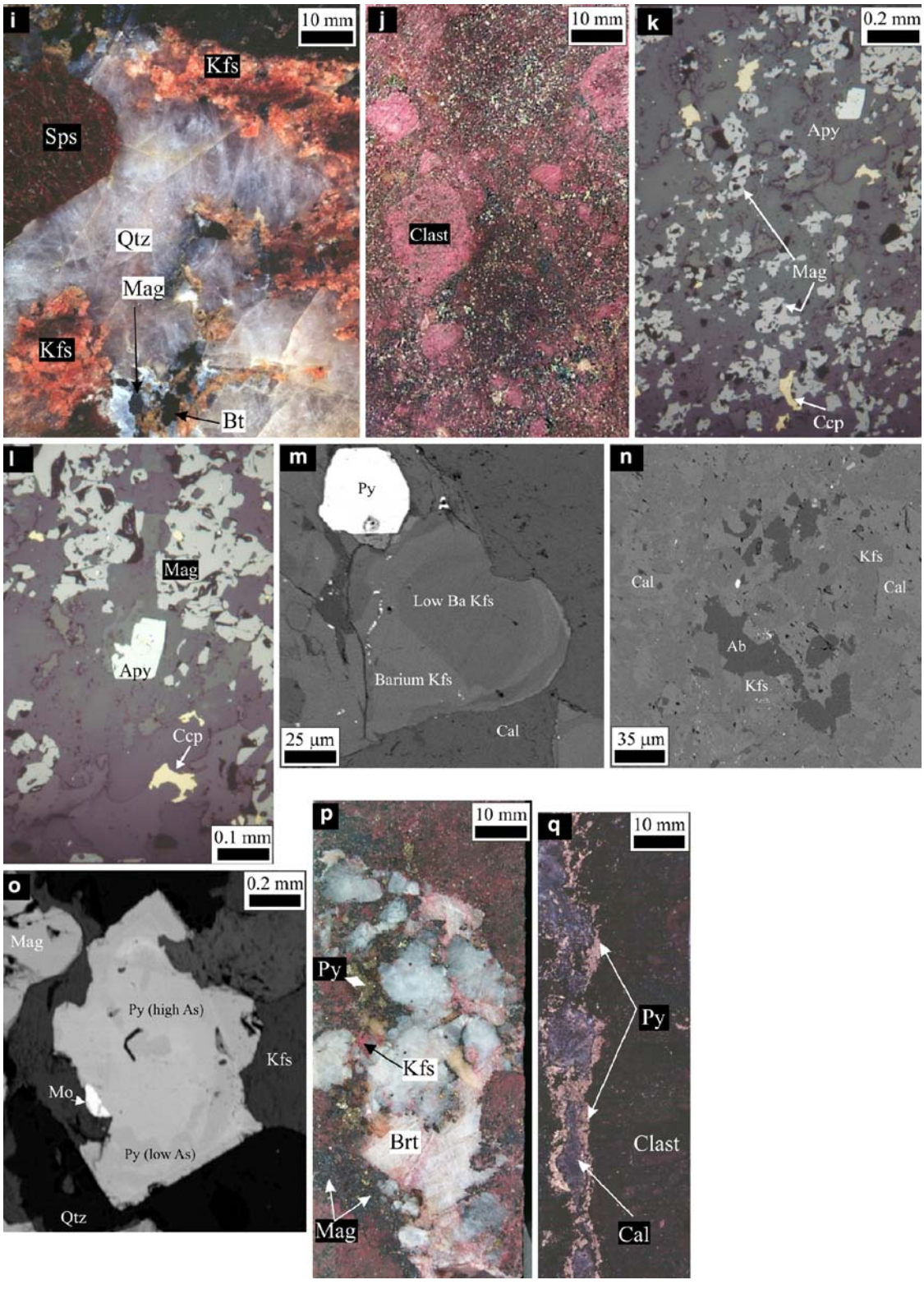

Fig. 5 (Contd.) (EH 141, 232.95 m). **o** Back scattered electron image of typical ore assemblage showing a zoned pyrite grain with few remaining euhedral grain boundaries, magnetite (Mag), K-feldspar (Kfs), quartz, pyrite (py) and molybdenite. The zonation in pyrite represents changes in the As, Co and Fe content, where the lighted shaded areas contain higher As and Co, at the expense of Fe and S (EH 141, 232.95 m). **p** Late coarse-grained veins composed of quartz, barite, K-feldspar, pyrite and chalcopyrite in ore breccia (FTCD 48, 410.1 m). **q** Late vein composed of calcite, actinolite and biotite associated with pyrite and biotite alteration in ore breccia from near the footwall contact of the deposit (EH 197, 266.2 m)

Geochemistry

Wholerock geochemistry around Ernest Henry was undertaken for three main reasons: (1) to assess the geochemical affects of K–(Mn–Ba) alteration; (2) to understand the relationships between regional and ore-related hydrothermal associations; and, (3) to constrain the spatial distribution of geochemical haloes associated with Cu–Au mineralization as a basis for developing 'vectors-to-ore' criteria. These results are based both on data from 1–3 m drill core samples from resource and sterilization drilling, and from detailed geochemical sampling of meta-igneous rocks and their K–(Mn–Ba) altered equivalents. Oliver et al. (2004) presented results of similar calculations for regional Na ± Ca alteration, including some samples near Ernest Henry. Their work demonstrated that the early sodic alteration near Ernest Henry occurred with low mobility of Al, Ga, Si, Ce and La (with Ti and Y probably also immobile, but showing large standard deviations). It resulted in the enrichment of Na, and depletion of K, Ba, Ca, Rb and Sr.

Geochemical mass balances for K–(Mn–Ba) alteration

Three pairs of unaltered and K–(Mn–Ba) altered rocks were selected to assess the geochemical changes using the isocon approach of Grant (1986) (Table 5; Figs. 6a–c and 7). Each pair represents adjacent samples of equivalent host rocks separated by an alteration front that is unaffected by later veining or metasomatism. Minimum and maximum isocon gradients were defined visually for each sample pair, and the field between the two is considered to define elements that were largely immobile during alteration (e.g. Ti, Al and Zr), whereas those outside this field were mobile and exhibit various enrichment or depletion patterns.

Biotite- and magnetite-rich alteration

Assessment of the geochemical affects of this alteration is based on analyses of partially albitized, medium-grained metadiorite and plagioclase phyric meta-andesite and their magnetite- and biotite-altered equivalents (Fig. 6a–b). The metadiorite predominantly retains its metamorphic mineralogy, and is composed of hornblende, plagioclase, magnetite and titanite, whereas the meta-andesite is largely composed of plagioclase, quartz and lesser biotite, K-feldspar and magnetite. The minimum and maximum isocon gradients indicate that alteration was associated with little, if any mass change. Zirconium, Ti, Al, Th, Nb, Si, LREE and HREE exhibit minimal change, whereas K, Rb, Ba, Zn, Cl, LOI, Mg, Fe, Co, Ni and V were enriched, and Na, Ca, Cu, P, U, Eu and As depleted. These changes correspond to biotite and magnetite replacement of primary igneous plagioclase, hornblende and biotite.

K-feldspar rich alteration

A K-feldspar–magnetite-altered plagioclase phyric meta-andesite and its unaltered equivalent was investigated to assess the mass changes linked to potassic alteration associated with Cu–Au mineralization (Fig. 6c). The results of the analysis show that Al, Zr, Ti, Si and Hf exhibit minimal change due to alteration, and most likely were immobile. K, Rb, Ba, Pb, Cu and

Table 2 Representative electron probe composition of hydrothermal garnet associated with pre-ore K-, Mn-, and Ba-rich veining and alteration

Stage 2								
Wt %								
SiO_2	36.54	36.72	36.86	37.06	36.81	37.07	37.41	36.67
Al_2O_3	20.56	19.84	20.58	20.29	18.81	18.41	18.70	18.29
FeO*	18.60	19.26	18.62	18.52	12.12	12.80	12.53	12.36
Fe_2O_3*	1.09	1.13	1.09	1.08	0.71	0.75	0.73	0.72
MnO	19.06	18.83	19.12	18.96	21.16	22.68	22.49	22.57
MgO	1.46	1.38	1.54	1.16	1.05	0.91	1.26	0.90
CaO	4.02	4.13	3.80	3.74	9.04	7.71	8.57	8.61
Total	101.33	101.28	101.61	100.81	99.70	100.33	101.69	100.12
No. of cations calculated on the basis of 12 O per unit formula								
^{T}Si	2.93	2.95	2.95	2.99	2.98	3.00	2.98	2.97
^{T}Al	0.07	0.05	0.05	0.01	0.02	0.00	0.02	0.03
Al^{VI}	1.87	1.83	1.89	1.92	1.77	1.76	1.73	1.72
Fe^{3+}	0.07	0.07	0.07	0.07	0.04	0.05	0.04	0.04
Fe^{2+}	1.25	1.30	1.25	1.25	0.82	0.87	0.83	0.84
Mg	0.18	0.17	0.18	0.14	0.13	0.11	0.15	0.11
Mn	1.30	1.28	1.30	1.30	1.45	1.56	1.52	1.55
Ca	0.35	0.36	0.33	0.32	0.78	0.67	0.73	0.75
Mole percent end members								
Almandine	40.7	41.8	40.8	41.5	25.8	27.1	25.8	25.8
Andradite	3.4	3.6	3.4	3.3	2.4	2.5	2.5	2.5
Grossular	7.9	7.9	7.3	7.4	22.3	18.4	20.1	20.5
Pyrope	5.7	5.3	6.0	4.6	4.0	3.4	4.6	3.4
Spessartine	42.3	41.4	42.5	43.1	45.6	48.6	46.9	47.8

Table 3 Representative electron probe composition of hydrothermal K-feldspar in pre-ore K-, Mn-, and Ba-rich veins, syn-ore veins distal to the deposit and the ore breccia

Wt %	Stage 2		K-feldspar alteration						Ore stage		
	Garnet-bearing		*Proximal*			*Distal*			*Breccia-vein infill*		
SiO_2	62.82	62.39	63.92	63.75	64.97	66.11	65.78	65.01	62.11	65.15	62.48
Al_2O_3	18.02	17.98	18.47	18.82	18.33	18.40	18.35	18.03	19.30	18.79	18.23
BaO	3.61	3.10	3.11	2.82	1.48	0.47	0.22	0.77	4.99	0.60	3.00
CaO	bd	bd	bd	bd	bd	bd	bd	bd	bd	bd	bd
Na_2O	0.75	0.99	0.30	0.66	0.52	bd	bd	0.22	1.20	0.00	1.34
K_2O	14.81	15.46	15.72	15.51	15.54	16.28	17.06	17.14	14.03	17.06	14.75
Total	100.01	99.92	101.52	101.56	100.84	101.26	101.41	101.17	101.63	101.60	99.80
No. of cations based on 16 oxygens											
Si	5.98	5.97	5.97	5.94	6.01	6.03	6.02	6.03	5.83	5.97	5.95
Al	2.02	2.03	2.03	2.06	2.00	1.98	1.98	1.97	2.14	2.03	2.05
Ba	0.14	0.12	0.11	0.10	0.05	0.02	0.01	0.03	0.19	0.02	0.11
Ca											
Na	0.14	0.18	0.05	0.12	0.09			0.04	0.22	0.00	0.25
K	1.80	1.89	1.87	1.84	1.83	1.89	1.99	2.03	1.68	2.00	1.79
Total	10.07	10.19	10.04	10.07	9.98	9.91	10.00	10.10	10.06	10.02	10.15

As were enriched, and Na, Ca, Sr, Co, Ni, REE, Y, LOI, P, Cl and Sb were depleted. These geochemical changes correlate to the breakdown of primary plagioclase, biotite and probably quartz and the formation of new K-(Ba)-feldspar, magnetite and minor pyrite. The trends here are similar to those for the earlier biotite and magnetite alteration, with notable exceptions being the enrichment of Cu and As and depletion of Co, Zn and Ni during K-feldspathization, the opposite trends shown by biotite and magnetite alteration.

Table 4 Average composition of hydrothermal biotite formed in early biotite–magnetite alteration, pre-ore K-, Mn-, and Ba-rich veins, syn-ore breccia and skarn

Wt %	Biotite–magnetite veining				Stage 2		Ore stage			
	Distal		*Proximal*		*Garnet-bearing veining*		*Breccia*		*Local skarn*	
	n = 5	*s.d.*	*n* = 6	*s.d.*	*n* = 8	*s.d.*	*n* = 7	*s.d.*	*n* = 14	*s.d.*
SiO_2	36.96	0.68	36.94	0.73	36.91	0.34	38.03	0.44	35.46	0.99
TiO_2	3.32	0.44	1.25	0.05	2.18	0.12	0.90	0.10	2.80	0.19
Al_2O_3	14.07	0.34	13.22	0.27	13.23	0.32	12.49	0.27	14.67	0.38
FeO	19.61	0.17	18.72	0.46	18.01	0.29	14.38	0.24	24.65	1.85
MnO	0.34	0.21	0.82	0.06	0.09	0.13	0.55	0.09	0.63	0.13
MgO	11.49	0.12	12.24	0.51	12.81	0.24	16.35	0.30	8.97	0.56
K_2O	9.70	0.18	10.28	0.16	10.11	0.15	9.81	0.28	9.76	0.70
F	bd	bd	1.58	0.08	0.43	0.07	1.45	0.11	0.91	0.82
Cl	0.64	0.08	0.26	0.03	0.63	0.07	0.49	0.08	0.89	0.06
H_2O	1.71	0.04	1.01	0.04	1.48	0.03	1.05	0.06	1.19	0.37
–O = F, Cl	0.15	0.02	0.73	0.04	0.33	0.02	0.72	0.05	0.59	0.35
Total	97.70		95.59		95.55		94.77		99.34	
No. of cations based on 24 oxygens										
Si	5.91	0.07	6.06	0.04	6.00	0.05	6.12	0.04	5.75	0.09
AlIV	2.09	0.07	1.94	0.04	2.00	0.05	1.88	0.04	2.25	0.09
AlVI	0.56	0.02	0.61	0.03	0.53	0.03	0.48	0.03	0.55	0.05
Ti	0.40	0.05	0.15	0.01	0.27	0.01	0.11	0.01	0.34	0.03
Fe^{2+}	2.62	0.02	2.57	0.09	2.45	0.05	1.94	0.04	3.34	0.26
Mn	0.05	0.03	0.11	0.01	0.01	0.02	0.08	0.01	0.09	0.02
Mg	2.74	0.07	2.99	0.09	3.10	0.05	3.92	0.07	2.17	0.12
K	1.98	0.04	2.15	0.05	2.10	0.03	2.01	0.05	2.02	0.13
Cations	16.35	0.06	16.58	0.04	16.53	0.05	16.65	0.04	16.52	0.03
F			1.64	0.09	0.45	0.07	1.48	0.11	0.93	0.84
Cl	0.35	0.04	0.15	0.02	0.35	0.04	0.27	0.04	0.49	0.04
OH	1.83	0.02	1.11	0.05	1.60	0.02	1.13	0.06	1.29	0.42

Table 5 Whole rock geochemistry of potassically - either biotite–magnetite (B-M), or K-feldspar (Kfs) - altered rocks and their precursor. The precursor rock for each pair is unaffected by potassic alteration or later hydrothermal products. Pairs of rocks are used to construct isocon diagrams (see Fig. 6) to assess the relative movement of elements during cycles of alteration. *Abbreviations:* A-D, albitized diorite; PPI, plagioclase phyric meta-andesite; Kfs, K-feldspar altered PPI; bd- below detection. Blank- element below detection in both samples

SAMPLE No.	J1L	J1M	X-factor	A27L	A27M	X-factor	G1ML	G1M1	X-factor
Rock Type	A-D	B-M	Isocon	PPI	B-M	Isocon	PPI	Kfs	Isocon
	Fig. 6a			Fig. 6b			Fig. 6c		
Wt %									
SiO_2	57.51	51.35	0.5	49.71	43.09	0.5	54.75	55.04	0.5
TiO_2	1.12	1.28	10	1.23	1.18	10	1.79	1.26	10
Al_2O_3	18.0	17.4	1	15.9	15.1	1	15.8	16.0	1
$Fe_2O_{3(t)}$	8.69	11.93	1	15.77	27.90	1	11.53	9.92	1
MnO	bd	0.06	100	0.14	0.12	100	0.09	0.09	100
MgO	2.28	5.26	5	0.85	1.31	5	2.34	bd	5
CaO	1.19	0.78	6	4.20	2.65	6	2.48	2.30	6
Na_2O	8.72	5.30	3	5.18	3.54	5	3.66	0.77	6
K_2O	1.01	4.38	5	3.75	3.96	2	5.84	12.47	2
P_2O_5	bd	bd		1.03	0.37	10	0.24	0.29	10
S	bd	bd		bd	0.01		bd	bd	
LOI	1.23	2.03	5	2.11	0.85	5	1.44	1.38	5
Total	99.8	99.8		99.9	100.0		100.0	99.5	
Parts per million									
Cl	337	573	0.05	31	41	0.5	197	125	0.1
Ba	193	909	0.01	398	405	0.01	1390	2488	0.01
Sr	104	224	0.1	72	55	0.3	83	45	0.3
Rb	49	266	0.1	83	133	0.2	146	296	0.05
Pb	3	bd	1	bd	bd		4	5	1
Th	16.6	17.4	1	8.9	7.1	1	21.4	13.5	0.5
U	4.45	3.09	3	bd	bd		6.25	5.86	1
Ta	bd	bd		1.08	bd	10	bd	bd	
Zr	163	192	0.1	169	161	0.1	323	297	0.05
Hf	6.54	9.06	2.0	4.01	4.21	2	7.73	6.92	1
Sb	0.68	0.52	10.0	0.66	0.37	10	0.79	0.37	5
Cs	bd	5	5.0	bd	bd		2.41	bd	10
Nb	13	14	1.0	10	7	2	19	10	1
Y	26	17	1.0	33	19	0.5	46	24	0.5
La	31	29.6	0.5	31.9	26.3	0.5	46.5	32	0.5
Ce	65.8	62.6	0.2	53.2	43.8	0.5	94.7	54.3	0.03
Sm	5.08	4.56	1	3.33	2.65	3	7.57	4.14	0.5
Eu	1.41	1.03	8	0.53	bd	8	2.00	1.03	2
Tb	0.81	0.74	8	0.52	bd	8	1.12	0.72	4
Yb	2.69	2.43	8	1.69	1.17	8	3.53	2.1	4
Lu	0.34	0.35	15	0.25	bd	15	0.49	0.29	15
Sc	4	4	1	18	27	1	19	4	1
Mn	259	487	0.05	1069	910	0.01	658	603	0.04
V	157	225	0.1	273	524	0.1	228	175	0.1
Cr	bd	19	1	14	10	1	bd	3	9
Co	7	17	1	10	29	1	17	4	1
Ni	24	48	0.5	34	59	0.5	33	15	0.8
As	2	1	10	6	4	1	1	3	10
Br	1.51	bd	15	bd	bd		bd	1.23	15
Cu	10	5	1	7	1	1	17	43	0.5
Zn	15	25	1	20	21	1	55	22	0.3
Mo	bd	7.4	1	5.7	bd	1	bd	bd	
Ga	26	31	0.8	21	27	1	24	17	1
W	bd	bd		bd	bd		bd	3	10
Sn	bd	9	1	bd	2	1	bd	bd	

Large-scale lithogeochemical patterns

Geochemical data from exploration drilling from 353 (1–3 m) drill core intervals at 1947 m RL (~200 m below the present surface) were used to assess the main element associations around the Ernest Henry deposit (cf. Fig. 8a–h). These data were also employed to construct element contour plots over a 16 km^2 plan section (~200 m below the surface) over the deposit to show the 2-D spatial relations of element distributions linked to hydrothermal alteration (Fig. 9a–h). Due to the presence of > 30 m of young cover over the Ernest Henry deposit, drill core data provides the only means to assess the geology and geochemistry of the Ernest Henry system. Data for geochemical contour plots for K, Ba and Na are available for the term lease only,

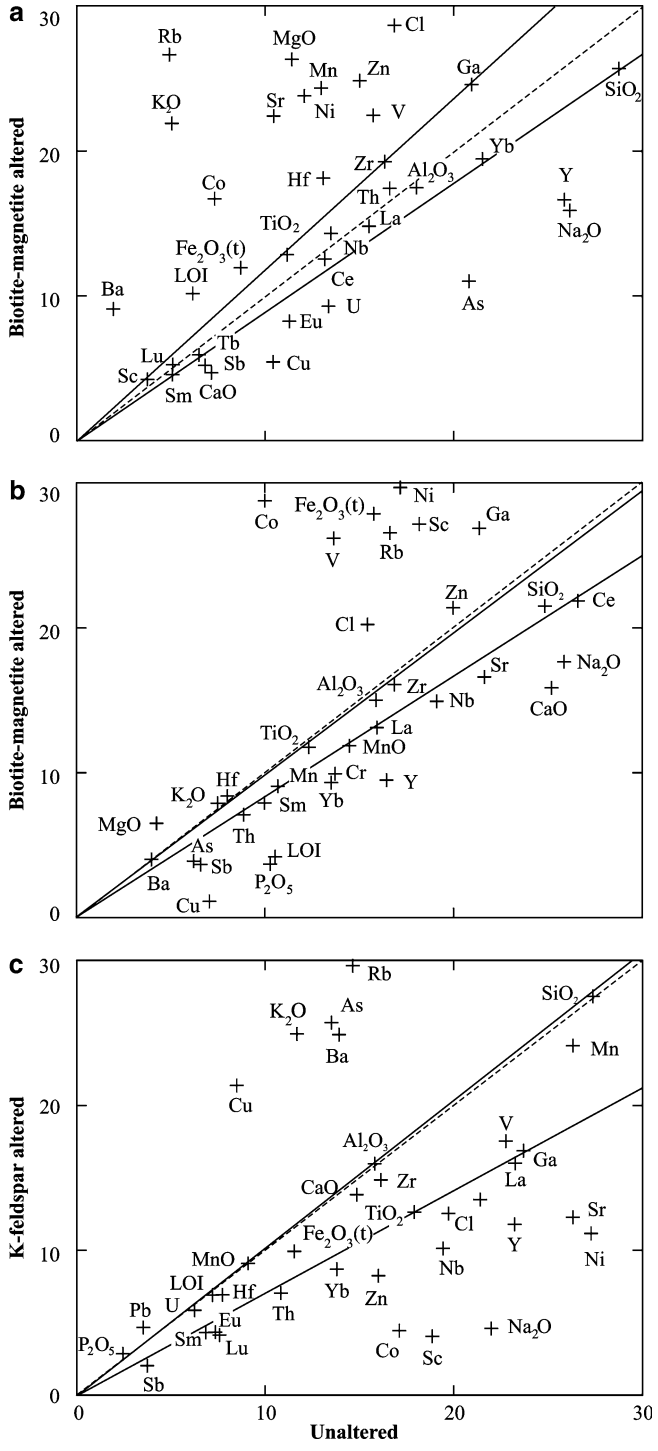

Fig. 6 Isocon plots (after the approach of Grant 1986) constructed for individual pairs of rocks (Table 5) comparing the effects of: **a** biotite–magnetite alteration (J1M) of partially albitized diorite (J1L) **b** biotite–magnetite alteration (A27M) on plagioclase phyric meta-andesite (A27L) and **c** K-feldspathization (G1M1) on plagioclase phyric meta-andesite (G1ML)

whereas Mn, Fe, U, As and Cu employ data from both the term and mine leases. Copper, Au, Fe, Mn, Co, U, and Ni were determined from whole rock samples from both the mine and term lease, whereas

Relative mass changes	K-feldspar alteration	Biotite-magnetite alteration
Increase	K, Rb, Ba, Pb Cu, As	K, Rb, Ba, Fe, Zn, Mg, Mn Co, Ni, V, Sc Ga, Hf, Cl
Decrease	Na, Ca, Sr, REE Co, Ni, Zn, Sb P, Y, Cl	Na, Ca, Sr, Eu Cu, U, As, Sb P, Y

Fig. 7 Diagram summarizing the generalized patterns of element behaviour linked to different styles of potassic alteration around Ernest Henry prior to Cu–Au mineralization

Ba, K and Na were only available for intervals outside the mine lease.

The Ba:K ratios are variable and in Fig. 8a exhibit a fan-like distribution, presumably due to the effects of: (a) variable Ba-content of K-feldspar (cf. Figs. 5m and 8a); (b) fluctuating abundances of hydrothermal biotite; and, (c) barite content. A strong antithetic association between K and Na is pronounced in rocks that contain elevated Na + K contents (>6 wt%). This pattern is less obvious in samples only partly affected by alkali feldspar alteration, mainly represented by rock suites containing <6 wt% (Na + K), and is most likely obscured by variations in the primary alkali distribution in the original host rocks.

Fe and Mn exhibit two main associations (Fig. 8c). Firstly, a weak positive Fe–Mn association occurs in rocks with low Fe and Cu, reflecting pre-ore biotite and/or garnet-rich alteration associations at the periphery of the deposit. Secondly, a poorly correlated high Fe-low Mn association occurs in ore breccia with >0.2 wt% Cu. Even though rocks in the alteration envelope around the orebody contain higher Mn, the ore has Mn-contents similar to or higher than average continental crust. Fe and Au data form two populations: one displays a positive correlation to high Cu (>0.1 ppm), while the other is a high Fe - low Au association (Fig. 8d). The occurrence of Fe-rich rocks with little Au and Cu reflects the presence of at least one generation of magnetite (± biotite) not associated with chalcopyrite, and may correlate with magnetite- and apatite-rich veining in the vicinity of the deposit.

A number of elements (e.g. Au, Cu, Ba, Mn, Fe, Co, As, U, Sb, Mo, Ag and Bi) exhibit significantly elevated concentrations compared to the average composition of felsic igneous rocks (cf. Berkman 1989). A coherent ~20000:1 correlation occurs between Cu and Au in rocks with >0.1 ppm Au (Fig. 8e). This Cu–Au association is consistent across the deposit, except in areas affected by supergene processes (cf. Gunton 1999). Supergene effects are essentially absent at the depth considered here. Strong associations between Cu, and elevated Co and As are particularly apparent in rocks with >0.2 wt% Cu, and are directly related to the close

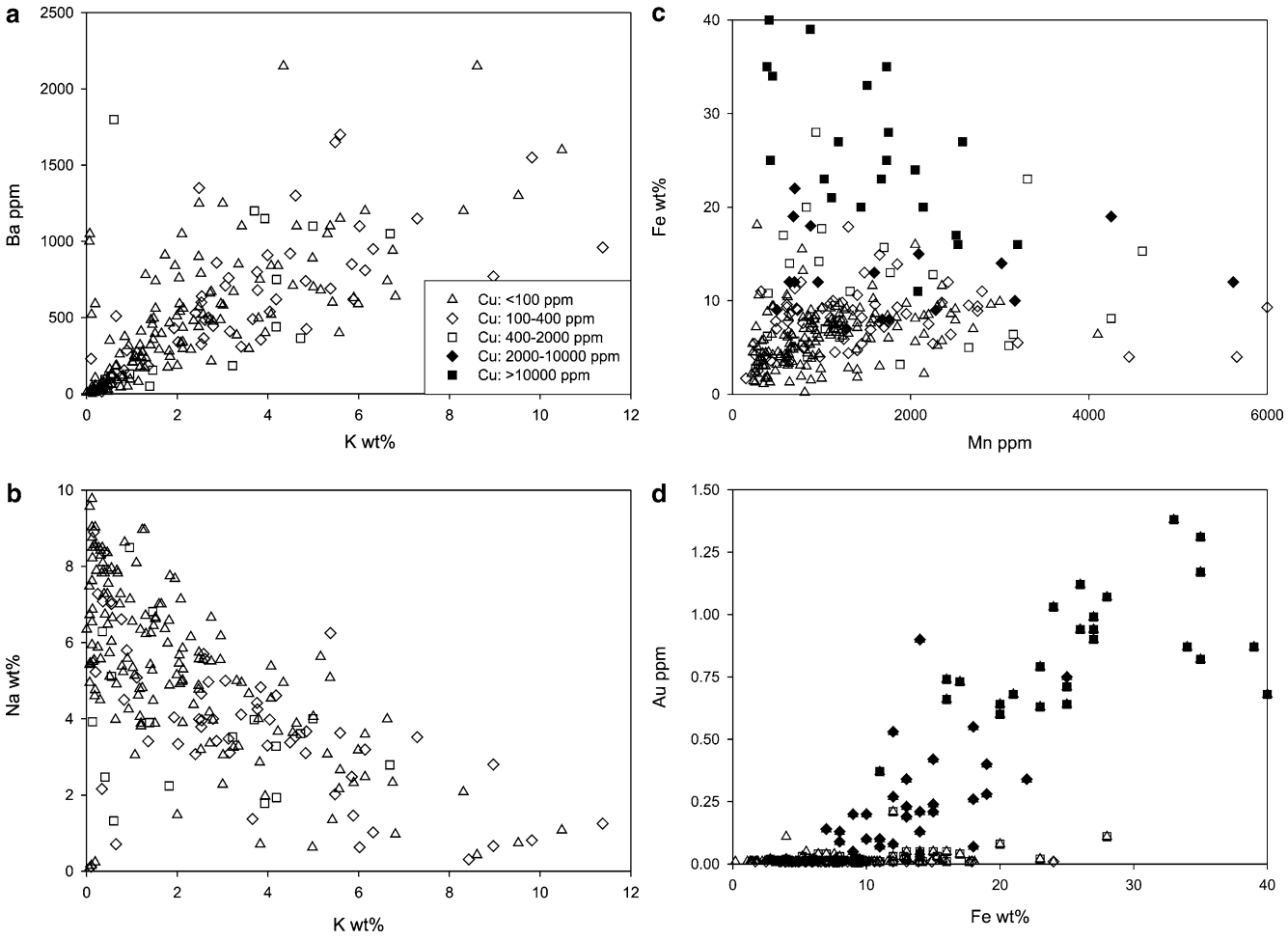

Fig. 8 Major and trace element plots showing the lithogeochemical relations between elements using whole rock data from drill core across the Ernest Henry term lease at 1947 m RL. Only data for Cu, As, Co, Mn, Fe, U and Ni are available for both the mine and term lease geochemical data sets. **a**: K vs Ba **b**: K vs Na **c**: Mn vs Fe **d**: Fe vs Au **e**: Au vs Cu **f**: Co vs Cu **g**: As vs Cu **h**: Ni vs Cu

relations between ore-stage arsenian-cobaltian pyrite, and chalcopyrite (Fig. 8f–g). The concentration of Ni in the ore at Ernest Henry is low compared to the pyrrhotite-rich ores of the Eloise, Osborne and Mount Elliott Cu–Au deposits (Adshead 1995; Baker 1998; Wang and Williams 1999) and exhibits no demonstrable correlation with Cu (Fig. 8h).

Geochemical footprint of hydrothermal alteration: spatial relations

A zone of high K (>6 wt%) extends for >1 km from the ore (Fig. 9a), correlating with biotite–magnetite, and later K-feldspar alteration assemblages. High K zones occur adjacent to the mine lease, and along the southwestern extension of the footwall shear zone and within parallel structures to the north and south. The distribution of elevated K correlates well with Ba (cf. Fig. 9a and b). Although no data are available within the mine lease, the increasing intensity of this alteration towards ore observed from geological logs (cf. Fig. 2c and d) can be used to imply that anomalous K continues into the lease. The antipathetic relationship between K and Na is also manifest by zones of high K and low Na, which commonly occur adjacent to areas of high Na (Fig. 9a and d). Evidently, Na–Ca alteration was more widespread than the K-(Mn–Ba) alteration linked to Cu–Au mineralization (cf. Fig. 7a–d).

A large zone of Mn-rich rocks envelopes the orebody (Fig. 9c). This correlates well with the extent of garnet- and biotite-rich veining and alteration (Fig. 2), and is reflected in the high Mn–Fe association observed in the element–element plots (Fig. 8). The greatest area of anomalously high Fe correlates to the orebody, although similar Fe-rich, but Cu-poor occurrences are associated with sulphide deficient, magnetite- and apatite-rich rocks and biotite–magnetite alteration (Fig. 9e). Anomalous Cu also occurs along a number of NE-trending structures and coincides with high K (Fig. 9h). Zones of high As also correlate well with Cu, and tend to increase in concentration towards the orebody (cf.

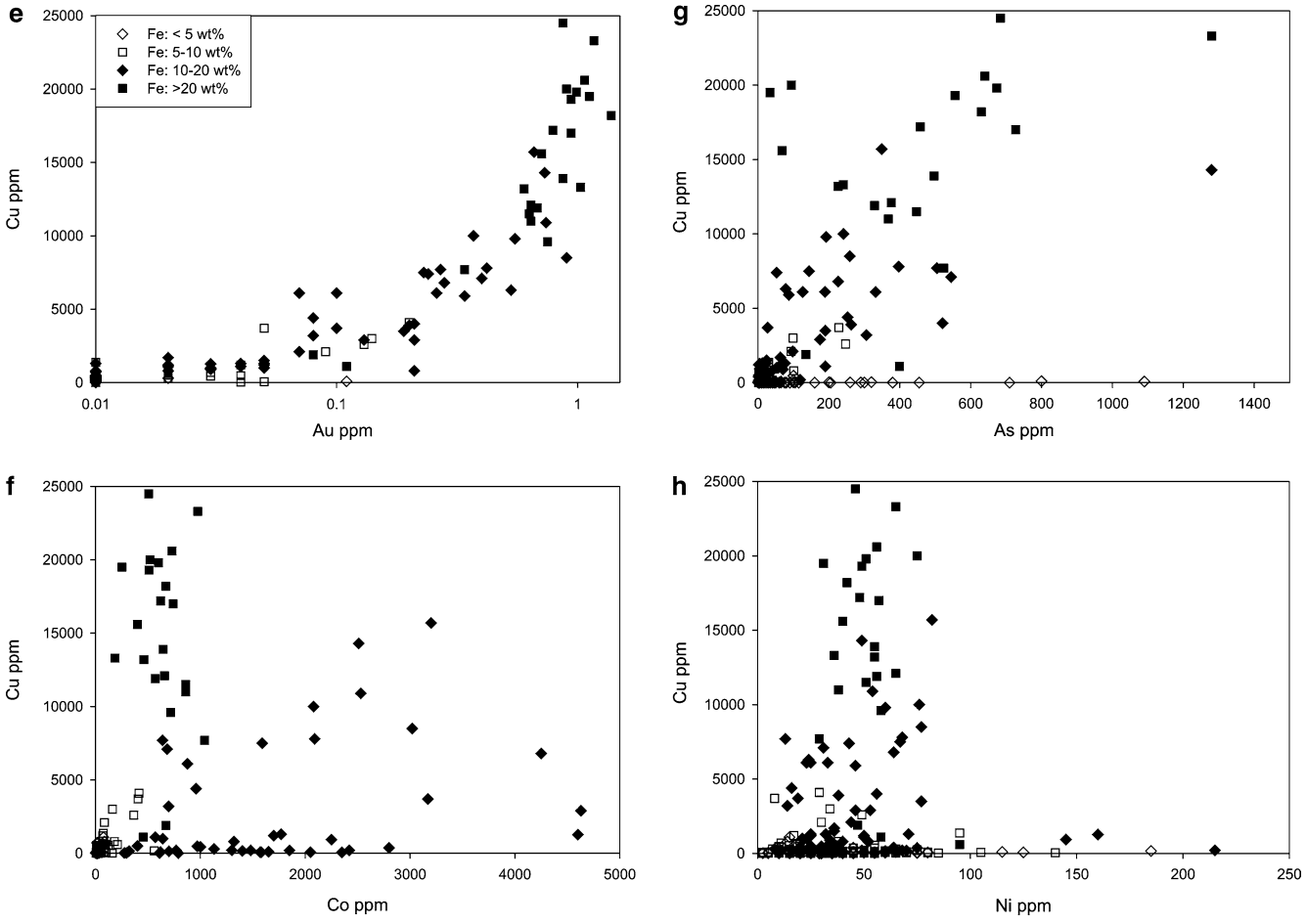

Fig. 8 (Contd.)

Fig. 9g and h). Rocks with high U cluster close to the orebody (Fig. 9f).

In summary, the spatial relations of geochemical features correlate well with the logged distribution and intensity of hydrothermal associations, and as such provide a number of km- (e.g. Mn, K, As and Co) and 100 m-scale (e.g. Fe, Cu and U) geochemical vectors towards the orebody.

Age of pre-ore alteration: U–Pb dating results

Previous geochronological studies (Twyerould 1997; Perkins and Wyborn 1998; Gunton 1999; Mark et al. 2004c) of the Ernest Henry hydrothermal system largely suggest that Cu–Au mineralization occurred sometime between 1.57 Ga and 1.47 Ga (Table 6). Cu–Au mineralization during this period indicates that ore deposition occurred after the metamorphic peak, and synchronously with the emplacement of the Williams and Naraku Batholiths (cf. Fig. 5). However, given the relatively imprecise timing of Cu–Au mineralization, together with the possibility that the Ar–Ar dates, particularly of biotite, may record much younger dates due to thermal resetting the age of the ore may be older. For example, at the Osborne deposit Re–Os dating of syn-ore molybdenite and U–Pb dating of pre-ore hydrothermal titanite return dates of ca 1.60 Ga for Cu–Au mineralization, whereas Ar–Ar dating of syn-ore biotite and amphibole for the same deposit return dates of ca 1.54 Ga (Table 6). As such, the timing and duration of the Ernest Henry hydrothermal system, particularly the relations between early phases of sodic and sodic–calcic alteration and ore deposition are relatively unconstrained. Consequently, we undertook U–Pb analysis of titanite from Ernest Henry by the Thermal Ionisation Mass Spectrometry (TIMS) method (cf. Fig. 5f) at Curtin University, Australia. Two titanite-bearing samples associated with early biotite and magnetite alteration and Na–Ca alteration were analysed. To avoid potential memory effects of earlier metamorphic or magmatic inheritance, only grains that represent the infill component to veins were selected for the analysis. Translucent to transparent titanite grains were separated by hand at James Cook University and were washed in de-ionised water. Grains were further cleaned, dissolved at the TIMS facility at Curtin University, and were spiked following the procedure of Pidgeon et al. (1996).

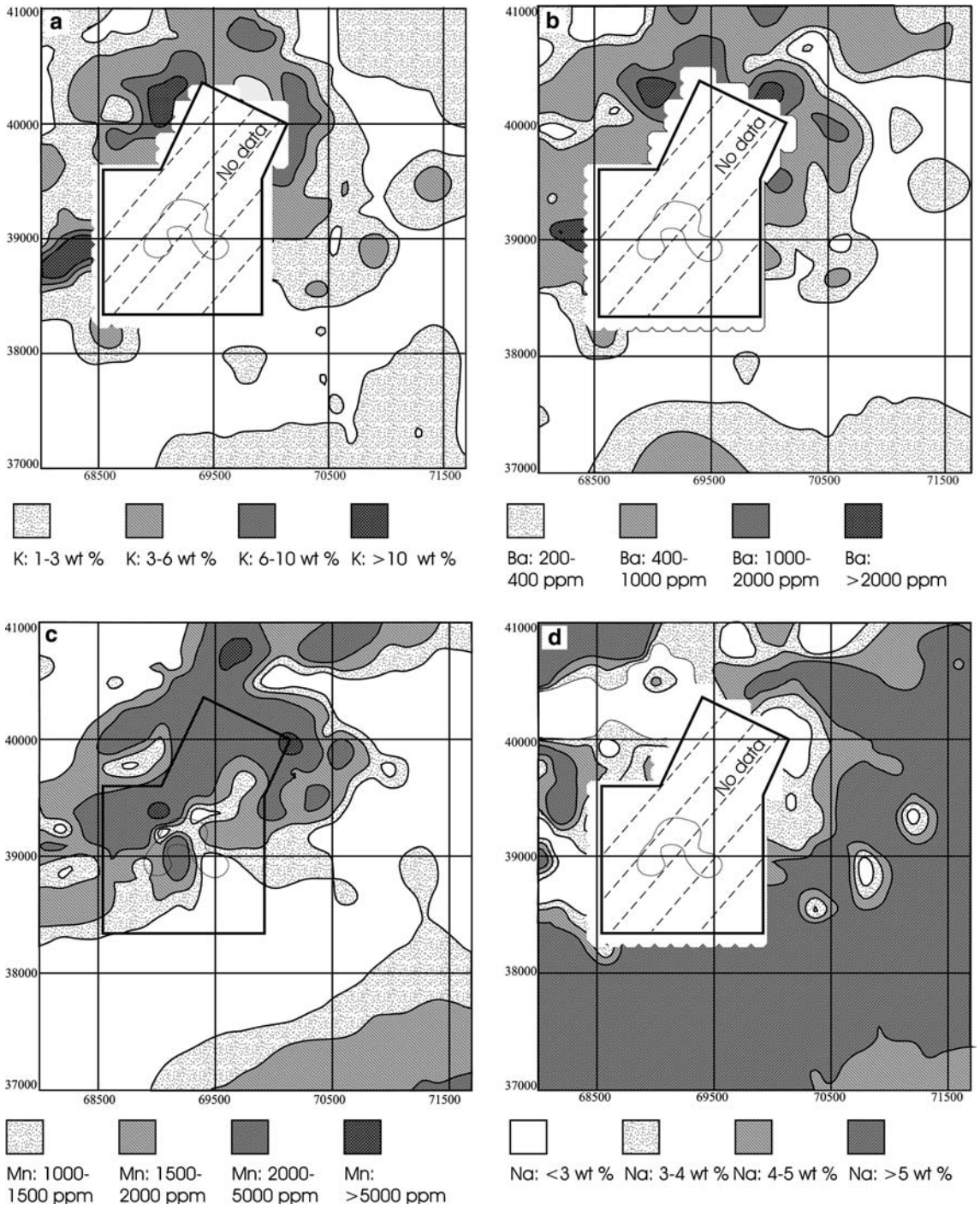

Fig. 9 Major element geochemistry of rocks within the term lease. These results are based on whole rock geochemical analysis of composite three meter drill intersections ca 1947 RL, or ca 200 m below the present level of exposure. Note that no data are available for K, Ba or Na within the mine lease, and thus the contours immediately adjacent to the mine lease boundary may exhibit some apparent distortion. The distribution of major and minor elements shown include: **a** K, **b** Ba, **c** Mn, **d** Na, **e** Fe, **f** U, **g** As; and, **h** Cu, and highlight the spatial relations between elements enriched during Cu–Au mineralization. These elements complement spatial relations between K-feldspar (K–Ba)–, garnet–biotite–magnetite–K-feldspar (Mn–Ba–K)– and albite (Na)-bearing hydrothermal alteration associations observed in core (cf. Fig. 2**b** and **c**). A strong antipathetic spatial association exists between areas affected by intense albitization and those overprinted by subsequent alteration related to Cu–Au mineralization. These data also provide a number of key geochemical criteria of particular interest to the explorationist (e.g. elevated K, Ba and Mn distal to Cu–Au mineralization)

The results of U–$Pb_{titanite}$ age determination (Table 7) indicate early Na–Ca alteration occurred at 1529 $+11/-8$ Ma, and pre-ore biotite–magnetite alteration at 1514 ± 24 Ma (Fig. 10a and b). These ages are indistinguishable within error, and are consistent with the post-peak metamorphic timing of hydrothermal alteration, as

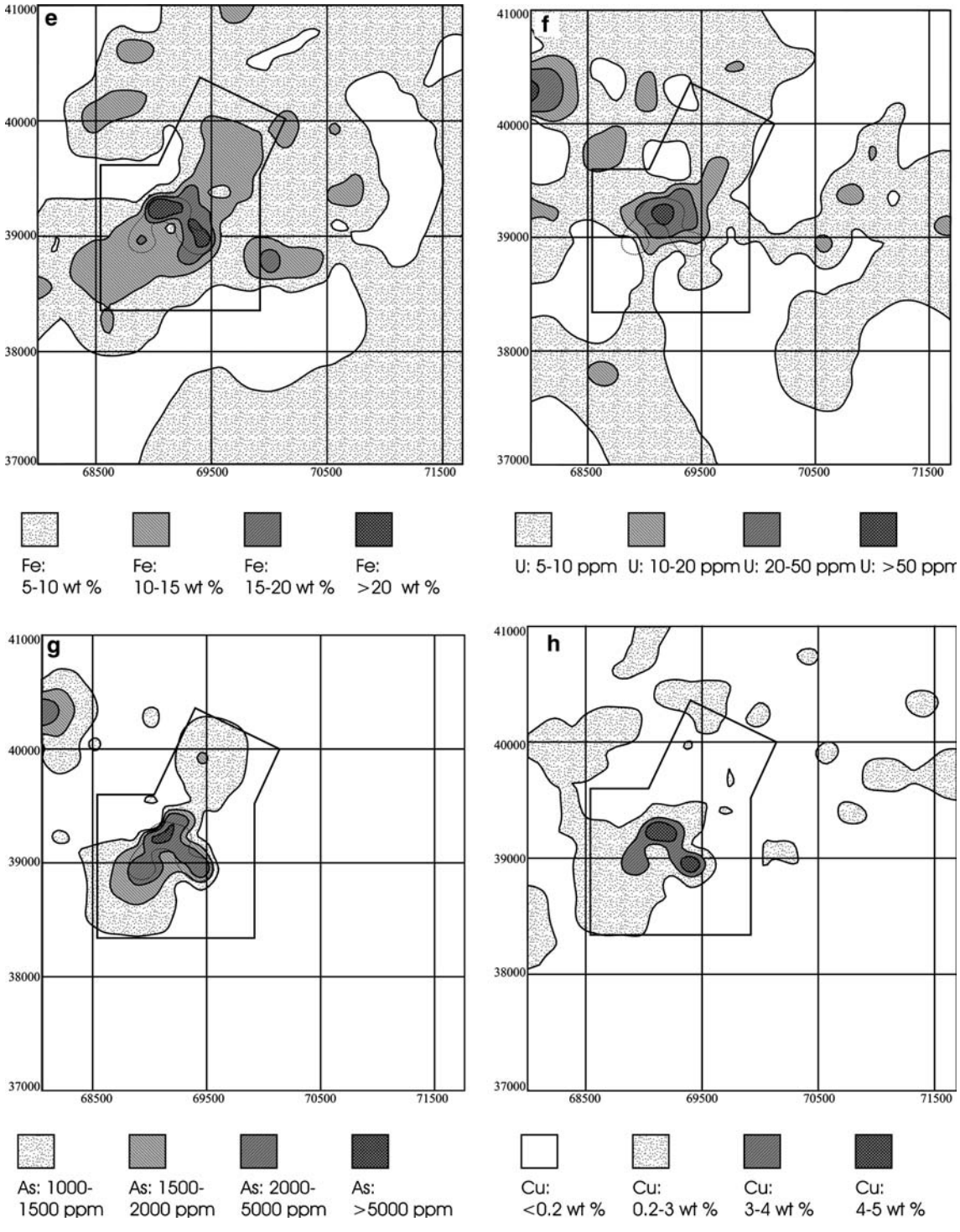

Fig. 9 (Contd.)

well as ca 1505 Ma (Ar–$Ar_{biotite}$, Twyerould 1997) and 1538 ± 37 Ma (Pb–Pb_{rutile}, Gunton 1999) ages for Cu–Au mineralization (cf. Table 7). These two new U–Pb ages also overlap with the emplacement age of the Williams and Naraku Batholiths, and more locally with the Mount Margaret Granite (ca 1530 Ma, Page and Sun 1998), the nearest-exposed granite, 15 km NE of Ernest Henry. Furthermore, these ages also overlap with ca 1525 Ma Re–Os ages for molybdenite in veins near to the ore deposit (cf. Mark et al. 2004c).

Table 6 Geochronological data for the timing of Cu-Au mineralization, granite intrusion, hydrothermal alteration, metamorphism and tectonism in the vicinity of Ernest Henry, northern Eastern Fold Belt

Hydrothermal System	^{40}Ar/^{39}Ar (Ma)	U–Pb (Ma)	Re–Os (Ma)	References
Ernest Henry Hydrothermal System:				
Early (?) Actinolite-magnetite veining (isochron age)	1610 ± 2			Twyerould 1997
Early (?) Actinolite-magnetite veining (isochron age)	1611 ± 4			Twyerould 1997
Late (?) Ferroactinolite-magnetite veining (isochron age)	1476 ± 3			Twyerould 1997
Biotite–Magnetite alteration: U–Pb: titanite		**1514 ± 24**		**This study**
Na–Ca alteration: U–Pb: titanite		**1529 ± 11/-8**		**This study**
Cu–Au mineralisation:1.^{40}Ar/^{39}Ar;biotite;U–Pb: rutile	1504 ± 3	1538 ± 37		Twyerould 1997;Gunton 1999
2. ^{40}Ar/^{39}Ar: biotite- ore stage	1476			Perkins and Wyborn 1998
Post-ore hydrothermal alteration, ^{40}Ar/^{39}Ar biotite	1514 ± 6			Twyerould 1997
Hydrothermal amphibole proximal to ore	ca 1526			Perkins and Wyborn 1998
Osborne Hydrothermal System				
Pre-ore ca-rich hydrothermal alteration:1. U–Pb: titanite	1595 ± 6			Gauthier et al. 2001
1. Ore stage:^{40}Ar/^{39}Ar: hornblende; Re–Os molybdenite	ca1540		1595 ± 6	Perkins and Wyborn 1998; Gauthier et al. 2001
2. Ore stage:^{40}Ar/^{39}Ar:biotite; Re–Os molybdenite	ca1540		1600 ± 6	Perkins and Wyborn 1998; Gauthier et al. 2001
Monakoff Cu–Au mineralization				
Ore stage: Ar: biotite	1508 ± 10			Pollard and Perkins 1997
Eloise Cu–Au Hydrothermal System				
Pre-ore biotite veining:^{40}Ar/^{39}Ar biotite	1555 ± 4			Baker et al. 2001
Stage 2 Hydrothermal veining:^{40}Ar/^{39}Ar hornblende	1530 ± 3			Baker et al. 2001
Stage 2 Hydrothermal veining:^{40}Ar/^{39}Ar hornblende	1530 ± 3			Baker et al. 2001
Stage 2 Hydrothermal veining:^{40}Ar/^{39}Ar biotite	1521 ± 3			Baker et al. 2001
Post-ore shear zone:^{40}Ar/^{39}Ar muscovite	1514 ± 3			Baker et al. 2001
Regional Na–Ca alteration				
Knobby albitite, Knobby Quarry		1555 ± 9		Oliver et al. 2004
Albitized breccia sheet, near knobby quarry		1521 ± 5		Oliver et al. 2004
Albitized breccia Cloncurry Fault		1524 ± 16		Oliver et al. 2004
Intrusive rocks north of Cloncurry				
Levian Granite: U–Pb zircon		1746 ± 8		Davis et al. 2001
Mount Fort Constantine volcanic rocks				
1. U–Pb zircon		1746 ± 9		Page and Sun 1998
2. U–Pb zircon		1742 ± 6		Page and Sun 1998
Ernest Henry diorite				
1. U–Pb titanite		1660 ± 13		Pollard and McNaughton 1997
2. U–Pb titanite		1658 ± 8		Pollard and McNaughton 1997
3. U–Pb titanite		1657 ± 7		Pollard and McNaughton 1997
Mount Margaret Granite				
1. U–Pb zircon		1530 ± 8		Page and Sun 1998
2. U–Pb zircon		1528 ± 6		Pollard and McNaughton 1997
Tea Tree Granite: U–Pb zircon		1512 ± 4		Pollard and McNaughton 1997
Malakoff Granite: U–Pb zircon		1505 ± 5		Pollard and McNaughton 1997
Mavis Granite: U–Pb zircon		1505 ± 5		Davis et al. 2001

Discussion

The new U–Pb$_{titanite}$ age data for early biotite–magnetite (1514 ± 24 Ma) and Na–Ca alteration (1529 + 11/−8 Ma) provide constraints that are relatively more resilient to thermal resetting as their blocking temperature (650–700°C: Frost et al. 2000, and references therein) exceeds the conditions of hydrothermal alteration (350–500°C) as well as the metamorphic peak (Foster 2003; Mark et al. 2005). Together with previous age dating, these data confine the earlier phases of the hydrothermal paragenesis to between 1,540 Ma and 1,500 Ma. The new U–Pb$_{titanite}$ data coincide with Ar–Ar dates determined by Perkins and Wyborn (1998) for amphibole (ca 1526 Ma) in massive carbonate in the footwall of the deposit, whereas Twyerould (1997) presented Ar–Ar data for hydrothermal amphibole in a skarn-type assemblage cutting the Ernest Henry diorite at 1476 ± 3 Ma (cf. Fig. 4). In contrast to these younger ages however, Twyerould (1997) also presented ca 1610 Ma Ar–Ar$_{amphibole}$ dates for actinolite–magnetite veining in the hanging wall of the deposit that indicate the presence of earlier alteration. Older ages are also recorded in a whole rock ore sample (Re–Os age: ca 1650 Ma) and in a single hydrothermal biotite (^{40}Ar–^{39}Ar spectra indicate a maximum age ca 1660 Ma) near the ore deposit, although the significance of these

Table 7 Titanite U–Pb TIMS isotopic data for early biotite and magnetite alteration, and later Na–Ca veining near Ernest Henry. Analyses were undertaken at Curtin University by Alexander Nemchin, and are corrected for blanks and common lead

Sample no.	Pb (ppm)	U	$^{206}Pb/^{204}Pb$	$^{207}Pb/^{206}Pb$	Error (%)	$^{207}Pb/^{235}U$	Error (%)	$^{206}Pb/^{238}U$	Error (%)	Corrected	$^{207}/^{206}$ age Ma	Error Ma
Biotite–magnetite												
a-1	7	17	159	0.09390	2.1	3.3351	2.7	0.2576	1.2	0.66	1506	40
a-2	7	19	155	0.09456	2.0	3.3320	2.4	0.2556	0.8	0.66	1519	37
a-3	9	23	190	0.09432	1.6	3.4655	1.9	0.2665	0.7	0.65	1515	30
Na–Ca alteration												
b-1	24	54	131	0.09516	2.3	3.4255	2.7	0.2611	0.5	0.88	1531	44
b-2	14	43	679	0.09507	0.4	3.4739	0.6	0.2650	0.3	0.67	1529	8
b-3	25	70	253	0.09272	1.2	3.3218	1.4	0.2598	0.4	0.70	1482	22
b-4	14	39	254	0.09431	1.2	3.2611	1.4	0.2508	0.5	0.66	1514	22
b-5	9	27	400	0.09571	0.7	3.3524	0.9	0.2540	0.4	0.65	1542	14
b-6	8	18	109	0.08273	5.3	2.7136	5.9	0.2379	1.2	0.64	1263	103

older ages to the genesis of the Ernest Henry hydrothermal system is yet to be fully explained (cf. Perkins and Wyborn 1998; Mark et al. 2004c). However, for the most part, the age dates from mineral separates formed during hydrothermal veining and alteration clearly are consistent with textural constraints for a post-peak metamorphic timing for the Ernest Henry hydrothermal alteration system (Table 6). Oliver et al. (2004) recorded $U–Pb_{titanite}$ ages for regional Na–Ca alteration of 1555 ± 9 Ma, 1527 ± 7, 1524 ± 16 Ma and 1521 ± 5 Ma, which, with the exception of the oldest of these from the Mary Kathleen Fold Belt 80 km west of Ernest Henry, are also indistinguishable from the new ages reported here. The 1540 to 1500 Ma age for Ernest Henry alteration and Cu–Au mineralization builds on the generally accepted timing of a major Cu–Au metallogenic period across the Cloncurry district. Ar–Ar ages for ore–related phases at other Cu–Au deposits include the Eloise (ca 1530–1512 Ma, Baker et al. 2001), Monakoff (ca 1508 Ma, Pollard and McNaughton 1997), Mount Elliott (1510 ± 3, Wang and Williams 2001) and Starra (ca 1503 Ma, Perkins and Wyborn 1998). Overall, the age constraints indicate that major hydrothermal activity commenced ca 1540–1530 Ma with Na–Ca alteration and early ore-related alteration, and cooled through the closure temperature of Ar–Ar systems in ore-related minerals in the range 1515 to <1505 Ma. These ages overlap with the emplacement of mid-crustal batholithic intrusions and regionally extensive Na–Ca alteration (cf. Table 6).

Fluid flow and the relations between hydrothermal alteration and Cu–Au mineralization

The rocks around the Ernest Henry mine preserve alteration patterns and paragenetic relations that show that Na–Ca altered (including albitized) rocks occur throughout the entire area, and are overprinted by K-(Mn–Ba) alteration and later breccia-hosted Fe oxide–Cu–Au mineralization. The chemical and temporal progression from sodic to potassic dominant alteration around the Ernest Henry deposit is also shared by many other Fe oxide Cu–Au districts formed during the Precambrian (e.g. Cloncurry district, Australia, Williams and Pollard 2003; Norrbotten County, Sweden, Edfelt and Martinsson 2003; Wanhainen et al. 2003; Carajás mineral province, northern Brazil, Requia et al. 2003) and Phanerozoic (e.g. Candelaria-Punta del Cobre and Manto Verde, Chile, Marschik and Fontboté 2001). The processes that caused these to evolve in this way are highly contentious, and are the subject of two main models:

1. *Fluid convection*: the alkali chemistry of alteration is envisaged to be controlled by the temperature-dependent nature of alkali exchange between alkali feldspar and aqueous fluid (cf. Orville 1963). This predicts that sodic alteration formed as a result of fluids being drawn towards a heat source (e.g. intrusion), whereas the same, but geochemically modified fluids produce potassic alteration in the cooling outflow zones of the same systems. Such large convection cells are related to many hydrothermal ore-systems in the shallow oceanic and continental crust, and have also been linked to hydrothermal alteration systems associated with porphyry-related systems (Carten 1985; Dilles et al. 1987). More recently, such processes have been proposed to operate in the hydrothermal systems hosting Fe oxide Cu–Au mineralization (Battles and Barton 1995; Barton and Johnson 1996).
2. *Single-pass hydrothermal systems (isothermal or cooling conditions)*: In these cases, initial Na–Ca alteration gives way to K–Fe alteration with time as a consequence either of temperature decreases or the change of fluid chemistry towards progressive K–Fe enrichment as Na and Ca are extracted from the fluid by wallrock interaction (e.g. Oliver et al. 2004). Such processes are problematic as they are limited to geological conditions that have starting fluid compositions with Na:K ratios higher than those in equilibrium with two feldspars (cf. Pollard 2001; Oliver et al. 2004). It has been speculated that such Na-rich fluids can be produced by CO_2 unmixing (cf.

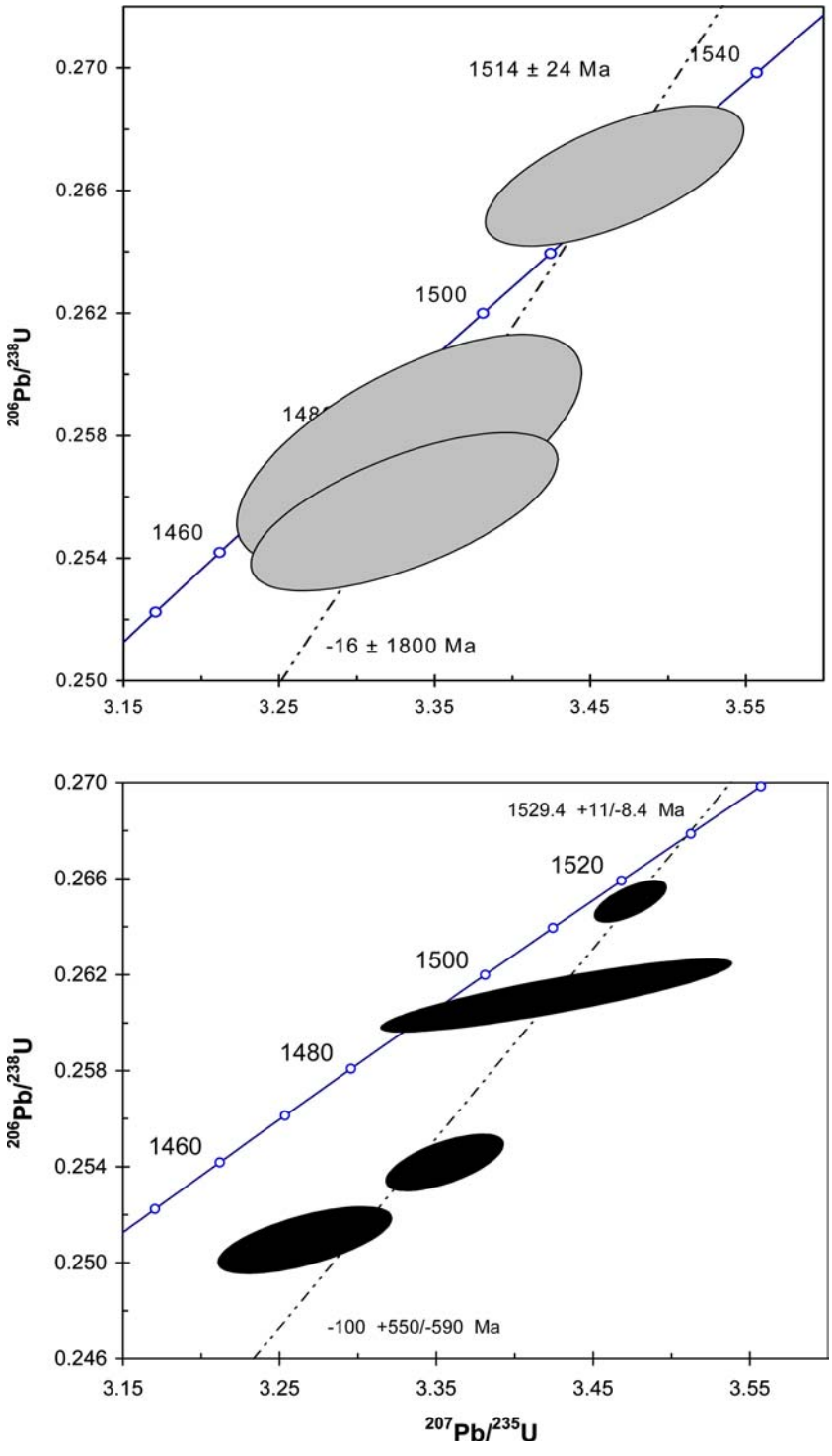

Fig. 10 U–Pb isochrons for titanites from two stages of hydrothermal alteration in the Ernest Henry hydrothermal system. Note that two data points, those that are discordant and which have markedly low Pb–Pb ages, were excluded in the calculation of the U–Pb concordia for Na–Ca alteration. **a** Early biotite and magnetite alteration. **b** Amphibole-rich vein associated with Na–Ca alteration (cf. Fig. 5f)

Pollard 2001), exsolution of magmatic fluids from K-deficient intrusions (Lang et al. 1995; Mark and Foster 2000), or via dissolution of halite-rich rocks (or their metamorphosed equivalents; cf. Oliver et al. 1993).

The Ernest Henry hydrothermal system appears to preserve evidence of two distinct cycles of metasomatism. Broadly, these two cycles are manifest by: (1) early sodic alteration, mainly as albitization, overprinted by hydrothermal biotite and magnetite, and (2) Multiphase Na–Ca veining and associated alteration overprinted by intense hydrothermal K-feldspar associated directly with the orebody. We speculate here on the possible interactions between these alteration phases by referring both to their spatial distribution and the geochemical and mineralogical changes. The early albitization appears to be similar in style and geochemistry to regional equivalents (Williams 1994; Mark 1998), with enrichment of

Na and depletion of K, Rb, Ba, Fe, Cl and Zn, and a distribution pattern also analogous to alteration observed on a regional scale. The biotite–magnetite alteration is broadly focussed around the orebody (at km scales), in a pattern dissimilar to the later K-feldspar alteration, which is even more closely related to ore (at 100 m scales). Thus, the outermost signal of the ore system appears to be the biotite–magnetite alteration, a pattern replicated around most of the other Cu–Au deposits in the district (Williams and Skirrow 2000). Both types of K-rich alteration involved enrichment in K, Rb, Zn, Ba and Fe, and depletion in Na and Ca, almost the opposite of that associated with Na and Na–Ca alteration (cf. Oliver et al. 2004). The complementary character of this mass exchange together with the temporal progression from Na-rich to K-rich alteration provides some support for a genetic association between the two types of alkali alteration, although in order for the alteration products to have been produced in the same system, the spatial relationships imply that the hydrothermal activity became progressively more focussed towards the vicinity of the orebody with time (cf. Fig. 11).

Oxygen and some hydrogen isotope data (Blake et al. 1997; Twyeroud 1997; Oliver et al. 2004) are available for minerals produced during most hydrothermal stages at Ernest Henry, and the results indicate a dominant magmatic–metamorphic contribution for fluids associated with Na–Ca alteration ($\delta^{18}O_{fluid}$ +7.9 to +11.5‰; δD_{fluid} −40 to −90‰), biotite–magnetite alteration distal to the ore ($\delta^{18}O_{fluid}$ +8.2 to +9.6‰; δD_{fluid} −44‰), later K-feldspar-rich alteration ($\delta^{18}O_{fluid}$ +6.7 to +10.5‰), and Cu–Au mineralization ($\delta^{18}O_{fluid}$ +7 to +12‰). These results are similar to those for regionally extensive Na–Ca alteration (Oliver et al. 1993; Mark and Foster 2000; Rubenach and Lewthwaite 2002; Marshall 2003; Mark et al. 2004a; Oliver et al. 2004; Marshall and Oliver 2005), as well as potassic alteration associated with other Cu–Au deposits in the district (Rotherham et al. 1998; Baker et al. 2001).

The involvement of fluids with a dominant magmatic component in pre-ore alteration at Ernest Henry appears to preclude the formation of coupled sodic and potassic alteration via convective hydrothermal circulation of shallow meteoric-formation waters immediately after the regional metamorphic peak (see also Pollard 2001). Consequently, the generation of early sodic and late potassic alteration in either of the two cycles described in the paragenesis at Ernest Henry requires either that (1) sodic and potassic alteration were coupled hydrothermal products ultimately sourced from sodic parent fluids that became progressively more K-rich via alkali exchange with K-bearing country rocks, or (2) the two types of alteration were derived from geochemically different, or evolving, sources. Alkali exchange via fluid-rock interaction is predicted in geochemical simulations of cooling or isothermal hydrothermal systems initially in equilibrium with granitic fluids (Oliver et al. 2004), where the igneous fluids probably derived their sodic character as a result of early CO_2 phase separation (cf. Pollard 2001). Thus, alkali exchange via fluid-rock interaction under isothermal or cooling conditions appears to provide a plausible scenario for drawing a link between the formation of early albitization and biotite–magnetite alteration at Ernest Henry. However, a similar scenario for the later cycle of sodic-calcic alteration and K-feldspar- and biotite-rich alteration immediately prior to ore deposition is probably unlikely because: (1) the volume and extreme magnitude of Ba and Mn enrichment associated with the potassic (K feldspar-rich) alteration is probably beyond the capacity of the country rocks to have sourced these components by simple mass exchange; and (2) the K-feldspar alteration was followed by enrichment of Cu and As (and Au) (Oliver et al. 2004). Consequently, we propose that even though a coupled association in a cooling or isothermal environment is probable for the early cycle of albitization and biotite–magnetite alteration at Ernest Henry, later Na–Ca alteration, and K-feldspar- and or biotite-rich alteration was most likely formed by other processes (Fig. 11).

Ore system geochemistry: insights into fluid origins and ore deposition

In hydrothermal systems, Fe solubility is largely controlled by fluid salinity and temperature (cf. Chou and Eugster 1977; Hemley et al. 1992; McPhail 1993; Sverjensky et al. 1997), although locally, rapid fluctuations in pressure (e.g. hydrothermal brecciation), reactive host-rock interaction, and changes in pH and/or redox via fluid mixing may also play a significant role. Iron enrichment at Ernest Henry is largely related to concentrations of magnetite, biotite and pyrite. Early Na–Ca alteration shows some relationship with magnetite–apatite–actinolite veins along structures in the hanging wall and footwall of the deposit, similar to many ironstone deposits that commonly reside within and proximal to sodically altered rocks (Badham 1978; Hildebrand 1986; Atkin et al. 1987; Vidal 1987; Williams 1994; Lang et al. 1995; Menard 1995; Edfelt and Martinsson 2003). In contrast, the Fe enrichment linked to potassic alteration occurs as zones of highly biotite ± magnetite altered rocks forming shear zones in the immediate hanging wall and footwall of the ore deposit, and as infill formed during Cu–Au mineralization. This Fe could have been derived by: (1) local scavenging from the country rocks as invoked for some sodic alteration systems (cf. Williams 1994; Lang et al. 1995; Menard 1995; Oliver et al. 2004); and/or (2) exsolution of fluids from contemporaneous magmas, as shown by Perring et al. (2000) at the granite hosted Lightning Creek magnetite deposit, Cloncurry district, and magnetite-rich skarn deposits elsewhere (Lentz et al. 1995; Kodera et al. 1998).

The simple mineralogy and dominant magmatic isotope signature (Blake et al. 1997) of the magnetite-apa-

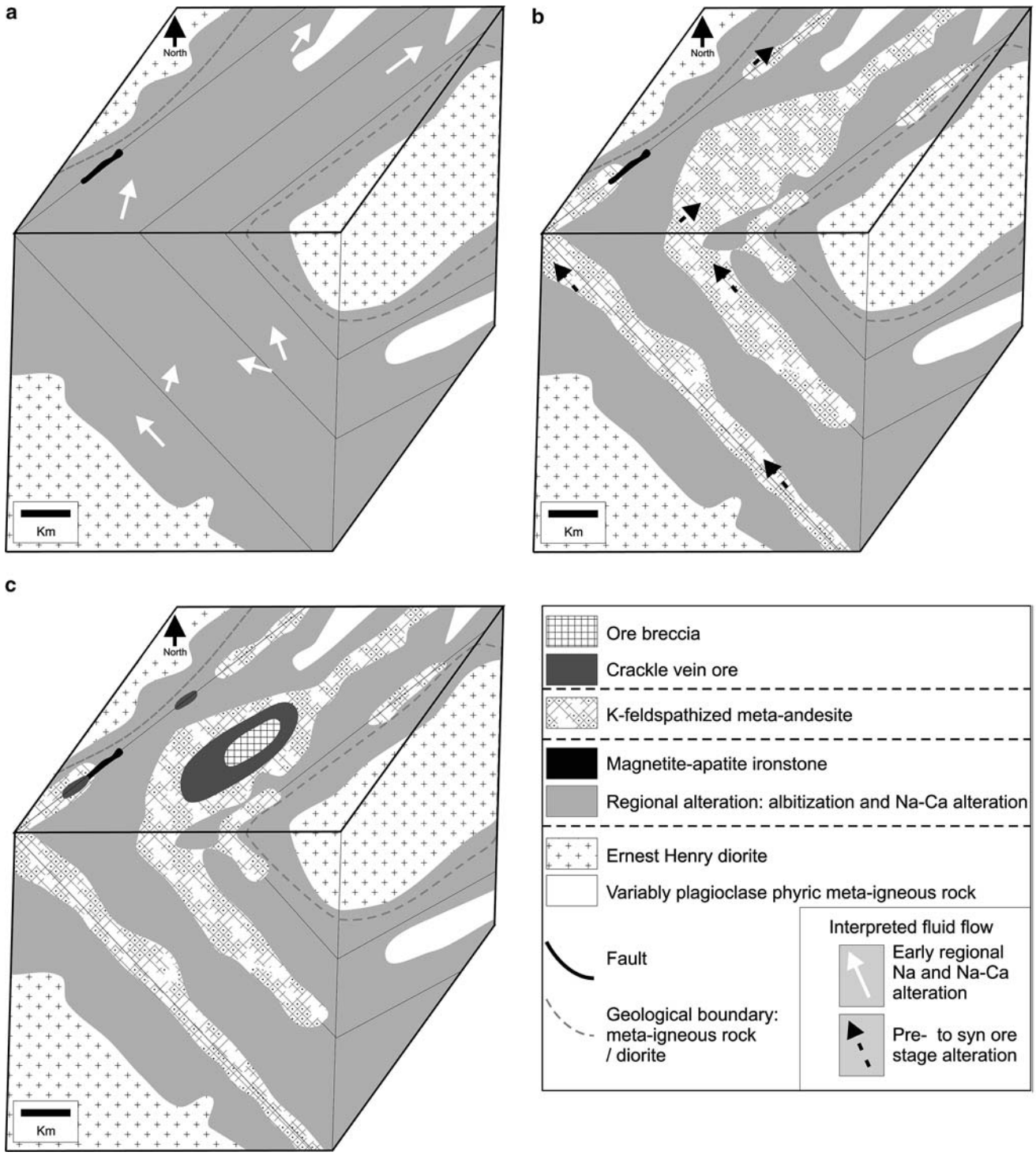

Fig. 11 Interpreted spatial and temporal evolution of the Ernest Henry hydrothermal system. **a** Early, structurally controlled pervasive albitization and Na–Ca alteration and localized brecciation hosted mainly along NE trending fluid conduits. **b** Pre-ore potassic alteration associated with Ba, Mn and Fe enrichment along NE trending footwall fluid conduits and the bounding shear zones hosting the orebody. **c** Localized dilation-induced hydrothermal brecciation and Cu–Au mineralization. Note minor occurrence of weak sulphide mineralization along some conduits other than those that host the orebody

tite veins at Ernest Henry indicates that they were probably formed as a result of cooling, wallrock reaction and potentially depressurization during fracture development. Biotite–magnetite alteration around the orebody may have shared this origin, because of the inverse relationship of the mass transfer with the earlier sodic alteration (cf. Oliver et al. 2004). In contrast, Fe enrichment in the matrix of the orebody coincides with enrichment of a diverse range of elements (e.g. Au, Mo, U, Co, As, Ag, Bi, W and Sn) that are absent or depleted

during earlier phases of alkali alteration (cf. Oliver et al. 2004). Some components were possibly carried together with the sulphur-bearing fluid that most likely mixed with the brine to induce sulphide precipitation. The presence of early sulphide-poor magnetite–apatite ironstones and later sulphide enriched Fe oxide Cu–Au mineralization at Ernest Henry is apparent in some other Fe oxide Cu–Au terranes (cf. Hitzman 2000; Edfeldt and Martinsson 2003). In the Ernest Henry hydrothermal system, the two types of ironstones exhibit distinctly different geochemical and mineralogical characteristics and are interpreted to have formed by different depositional mechanisms. We cannot completely rule out a genetic connection between the early biotite–magnetite alteration and the later ore because of the strong spatial association and the coincidence of at least some geochemical enrichment trends.

Significance of coincident Fe, K, Mn and Ba enrichment

The Ernest Henry hydrothermal system is characterized by a large Mn and Ba anomaly that is most pronounced in the footwall, and extends for >1 km from the deposit. High Ba and Mn is also associated with pronounced Fe and K enrichment reflecting the distribution of pre- and syn-ore spessartine-almandine, K(–Ba)–feldspar (up to 6 wt% Ba), barite, Mn-rich biotite (up to 1 wt% Mn) and magnetite. The appreciable Mn, Fe, K and Ba enrichment associated with Cu–Au mineralization at Ernest Henry is also apparent within the altered host rocks at the Monakoff Cu–Au deposit (Fig. 1), although Davidson et al. (2002) suggested that Mn, Fe, K and Ba enrichment in the latter deposit formed during two periods of quite separate hydrothermal alteration. Garnet from Monakoff and Ernest Henry exhibit similar geochemical characteristics, and bear some similarity to garnet-bearing rocks associated with hydrothermal alteration at the Cannington Ag–Pb–Zn deposit (cf. Chapman and Williams 1998; Davidson et al. 2002). The Aitik and Nautanen Cu–Au deposits in the Norrbotten Fe oxide Cu–Au terrane of Sweden share similar geochemical associations manifest by the presence of abundant garnet and K(–Ba)–feldspar in the vicinity of Cu–Au mineralization (Martinsson and Wanhainen 2000; Bergman et al. 2001). The coincidence of high K and Fe, and Mn and Ba in these ore-related hydrothermal systems is a geochemical feature that is typically decoupled in other ore systems, where many Cu–Au systems are invariably associated with coincident enrichment of K and Fe, but not Mn (cf. Proffett 2003; Seedorf and Einaudi 2004). Mn enrichment is commonly found in association with distal Zn-bearing skarns deficient in Ba (Einaudi et al. 1981; Williams and Heineman 1993; Chapman and Williams 1998; Baker et al. 2004).

The high concentration of Ba at the Ernest Henry deposit indicates that the ore fluids contained little sulphate, unlike typical Cu–Au porphyry fluids (cf. Ulrich et al. 2001), whereas the high Mn-content of the Ernest Henry ore envelope also indicates to fluids with unusually high Mn:Fe ratios. No published data are available on the composition and origin of fluids responsible for Mn and Ba enrichment. However, under the magnetite-stable, high temperature conditions interpreted for Ernest Henry thermodynamic data indicate that these cations are highly soluble in solution (Sverjensky et al. 1991). Analyses of magmatic fluids shows that high-temperature brines can contain high Mn and/or Ba, but both are typically not detected in high concentrations together (cf. Bottrell and Yardley 1988; Rankin 1992; Audétat et al. 2000; Perring et al. 2000; Ulrich et al. 2001). Geochemical data for brine inclusions associated with magnetite ironstone formation and later Au–Cu mineralization at the Starra deposit show that brines representing both of the hydrothermal stages contain high Mn and Ba, although those related to Au–Cu mineralization contain appreciably higher Ba (potentially as much as 10 wt%) and Mn (1.0–2.4 wt%: Williams et al. 2001). Williams et al. (2001) suggested as one possibility the origin of the brines to high-Ba intermediate intrusions.

Ore deposition via fluid mixing

The Ernest Henry ore breccia is enriched in a diverse suite of elements (e.g. Cu, Au, Fe, K, S, Ba, Ca, As, Co, Mo, U, F, REE, Bi, Ag, Bi, W and Sn) that are likely to have been carried as various chloride (e.g. Cu, Fe, Au, Co), CO_3^{2-} (e.g. U, REE) and hydroxide complexes (e.g. W and Mo). As the stability of these different complexes is affected by fluctuations in different physico-chemical parameters (e.g. Δ T, Δ P, Δ salinity, Δ pH, ΔfO_2) it is likely that more than one fluid was required to carry these components to the site of ore deposition, and that element enrichment occurred due to significant changes in many physico-chemical parameters during ore deposition. For example, given the low solubility of fluorite in hydrothermal solutions compared to its constituent ions (Richardson and Holland 1979), and the low solubility of barite in relatively oxidized (e.g. hematite-stable) solutions it is likely that F and Ca, and Ba and sulphur were carried by separate fluids prior to ore deposition. The origin of these separate fluids is yet to be fully explored. The presence of high temperature, (ca 375 ± 50°C), high salinity (35–55 wt% $NaCl_{equiv}$) brines trapped in syn-ore quartz (Mark et al. 2000) suggests that a significant proportion of base metals were probably carried as chloride complexes, and as such, ore deposition was likely to have occurred via cooling, decreasing pressure and/or dilution via fluid mixing. The relative paucity of syn-ore quartz in the breccia and little intragrain variation in ore pyrite $\delta^{34}S$ (cf. Mark et al. 2004d) also provides supporting evidence that cooling was probably not significant. Therefore, in order to most efficiently accommodate these observations, a model involving synchronous dilation, brecciation and fluid-mixing is suggested. However, even though the deposit is predominantly characterized as a

hydrothermal breccia enriched in a range of elements, apart from the presence of rare tiny inclusions (< 10 mm) of galena and sphalerite in the ore, both Pb and Zn are largely depleted during early albitization (cf. Oliver et al. 2004) and K-feldspar alteration (Fig. 6a–c). The absence of significant concentrations of Pb and Zn in the ore breccia probably indicates they remained soluble in the ore fluid, which is consistent with their higher solubility compared to Cu (e.g. Hemley et al. 1992). A potentially similar scenario has been documented in cooling porphyry systems (e.g. Bajo de la Alumbrera) where Pb and Zn remain in the spent solution after Cu–Au mineralization (Ulrich et al. 2001).

Geochemical and geophysical characteristics: uses in exploration

Empirical data from this study show that the Ernest Henry hydrothermal system produced a number of geochemically discrete alteration shells corresponding to mineral distributions that progress from: (1) a distal Mn, K and Ba enriched, and Na depleted shell > 1.0 km from the orebody; (2) an inner shell also enriched in As, Co and Cu up to 1.0 km from the orebody; and, (3) a proximal shell enriched in K, Fe, Cu, Au Mo, Ag, U, Sb and Bi up to 100s m from ore. This zonation would be expected to correspond to changes in the geophysical characteristics of the ore system where the proximal shell would form a magnetic and radiometric (K, U, Th) high, whereas the distal shell and orebody are likely to exhibit much higher magnetic responses that correlate with a moderate radiometric intensity with higher K:U ratios in which total counts would be anticipated to decrease with distance from the orebody. These characteristics and spatial relations can be used to help predict the range of geophysical responses expected from Fe oxide–Cu–Au systems from those similar to Ernest Henry, to those such as the Olympic Dam and Sue-Dianne deposits, which were formed under different geological conditions (e.g. T and fO_2) where hematite and/or muscovite are more abundant (cf. Goad et al. 2000).

Acknowledgements GM was supported by a Monash University Logan Fellow. The authors would like to gratefully acknowledge the financial and logistical support provided by Ernest Henry Mining Pty Ltd and MIM Exploration (now Xstrata Exploration). Financial assistance was also provided through an ARC SPIRT Grant C00002502. The authors would like to thank Richard Crookes, Max Alyffe, Joshua Bryant, Stewart Coates, Anne Hollonds and Max Tuesley (all formerly from Ernest Henry Mining Pty Ltd), and the rest of the technical staff in the Ernest Henry geology department headed by Perry Collier for their help and advise during the project. We are also appreciative of the guidance imparted by Rick Valenta. Roger Skirrow and an anonymous reviewer are recognized for their thoughtful and considered reviews. Kevin Blake from the Advanced Analytical Centre, James Cook University is also acknowledged for his technical know-how in electron probe microanalysis. Damien Foster, Brad Drabsch, Haidi Hancock and Justin Tolman are thanked for their help in sample preparation at James Cook University.

References

Adshead ND (1995) Geology, alteration and geochemistry of the Osborne Cu–Au deposit, Cloncurry district, NW Queensland. PhD thesis, unpublished. James Cook University

Adshead ND (1996) The role of hypersaline hydrothermal fluids in the formation of the Osborne Cu–Au deposit, Cloncurry district, NW Queensland. EGRU Contrib 55:1–4

Aitkin BP, Injque-Espinoza JL, Harvey PK (1985) Cu–Fe-amphibole mineralization in the Arequipa segment. In: Pitcher WS et al (eds) Magmatism at a plate edge: the Peruvian Andes. Blackie, Glasgow, pp 261–270

Audétat A, Günthur D, Heinrich CA (2000) Magmatic-hydrothermal evolution in a fractionating granite: a microchemical study of the Sn-W-F-mineralized Mole Granite (Australia). Econ Geol 95:1563–1581

Badham JPN (1978) Magnetite-apatite-amphibole-uranium and silver-arsenide mineralizations in Lower Proterozoic igneous rocks, East Arm, Great Slave Lake, Canada. Econ Geol 73:1474–1491

Baker T (1996) The geology and genesis of the Eloise Cu–Au deposit, Cloncurry district, Queensland, Australia. PhD thesis, unpublished. James Cook University

Baker T (1998) Alteration, mineralization and fluid evolution at the Eloise Cu–Au deposit, Cloncurry district, NW Queensland. Econ Geol 93:1213–1236

Baker T, Perkins C, Blake KL, Williams PJ (2001) Radiogenic and stable isotope constraints on the genesis of the Eloise Cu–Au deposit, Cloncurry district, NW Queensland. Econ Geol 96:723–742

Baker T, vanAchterberg E, Ryan CG, Lang JR (2004) Composition and evolution of ore fluids in a magmatic-hydrothermal skarn deposit. Geol 32:117–120

Barton MD, Johnson DA (1996) Evaporitic-source model for igneous-related Fe oxide-(REE-Cu–Au–U) mineralization. Geol 24:259–262

Barton MD, Johnson DA (2000) Alternative brine sources for Fe oxide–(–Cu–Au) systems: Implication for hydrothermal alteration and metals. In: Porter TM (ed) Hydrothermal Iron Oxide Copper-Gold and Related Deposits: A Global Perspective. AMF, pp 27–42

Battles DA, Barton MD (1995) Arc-related sodic hydrothermal alteration in the western United States. Geology 23:913–916

Bergman S, Kübler L, Martinsson O (2001) Description of regional geological and geophysical maps of northern Norrbotten county (east of Caledonian orogen). Geological Survey Sweden 56:110

Berkman DA (1989) Field geologist's manual. Australasian Institute of Mining and Metallurgy. AUSIMM Monograph Series 9:390

Blake DH (1987) Geology of the Mount Isa Inlier and environs. Queensland and Northern Territory. BMR Geol Geophys Bull 225:83

Blake K, Pollard PJ, Xu G (1997) Alteration and mineralisation in the Mount Fort Constantine volcanics, Cloncurry district, northwest Queensland. In: Pollard PJ (eds) Cloncurry base metals and gold. AMIRA P438 Final Report 11:53

Bottrell SH, Yardley BWD (1988) The composition of a primary granite-derived ore fluid from S.W. England, determined by fluid inclusion studies. Geochem Cosmochim Acta 52:585–588

Chapman LH, Williams PJ (1998) Evolution of pyroxene-pyroxenoid-garnet alteration at the Cannington Ag–Pb–Zn deposit, Cloncurry District, Queensland, Australia. Econ Geol 93:1390–1405

Chou I-M, Eugster HP (1977) Solubility of magnetite in supercritical chloride solutions. Am J Sci 277:1296–1314

Davidson GJ (1998) Variation in copper-gold styles through time in the Proterozoic Cloncurry Goldfield, Mt Isa Inlier: a reconnaissance view. Aust J Earth Sci 45:445–462

Davidson GJ, Davis BK, Garner A (2002) Structural and geochemical constraints on the emplacement of the Monakoff oxide Cu–Au (–Co–U–REE–Ag–Zn–Pb) deposit, Mt Isa Inlier. In: Potter TM (ed) Hydrothermal Iron oxide copper-gold and related deposits: a global perspective 2, pp 49–76

Davis BK, Pollard PJ, Lally JH, McNaughton NJ, Blake K, Williams PJ (2001) Deformation history of the Naraku Batholith, Mt Isa Inlier, Australia: implication for pluton ages and geometries from structural study of the Dipvale Granodiorite and Levian Granite. Aust J Earth Sci 48:113–129

Dilles JH, Farmer GL, Field CW (1995) Sodium-calcium alteration by non-magmatic saline fluids in porphyry copper deposits: Results from Yerington, Nevada. In: Thompson JFH (ed) Magmas, fluids and ore deposits. Mineralogical Association of Canada Short Course Series 23:309–338

Edfelt A, Martinsson O (2003) The Tjarrojakka Fe-oxide Cu (–Au) occurrence, Kiruna area, northern Sweden. In: Eliopoulos et al (eds) Mineral Exploration and Sustainable Development. Millpress, Rotterdam, pp 1069–1072

Einaudi MT, Meinert LD, Newberry RJ (1981) Skarn deposits. In: Skinner BJ (ed) Economic Geology 75th Anniversary Volume 1981, pp 317–391

Foster DRW (2003) Proterozoic low-pressure metamorphism in the Mount Isa Inlier, northwest Queensland, Australia, with particular emphasis on the use of calcic amphibole chemistry as temperature-pressure indicators. PhD thesis, unpublished. James Cook University

Frost BR, Chamberlain KR, Schumacher JC (2000) Sphene (titanite): Phase relations and role as a geochronometer. Chem Geol 172:131–148

Gauthier L, Hall G, Stein H, Schaltegger U (2001) The Osborne deposit, Cloncurry district: a 1595 Ma Cu–Au skarn deposit. In: Williams PJ (ed) 2001 a hydrothermal odyssey, new developments in metalliferous hydrothermal systems research, extended conference abstracts. EGRU 59:58–59

Giles D, Nutman AP (2002) SHRIMP U–Pb monazite dating of 1600–1580 Ma amphibolite facies metamorphism in the southeastern Mt Isa Block, Australia. Aust J Earth Sci 49:455–465

Goad RE, Hamid Mumin A, Duke NA, Neale KL, Mulligan DL (2000) Geology of the Proterozoic Iron Oxide-Hosted, NICO Cobalt-Gold-Bismuth, and Sue-Dianne Copper-Silver deposits, Southern Great Bear Magmatic Zone, Northwest Territories, Canada. In: Porter TM (ed) Hydrothermal Iron Oxide Copper-Gold and Related Deposits. A Global Perspective. AMF, pp 249–268

Grant JA (1986) The isocon diagram- a simple solution to Gresen's equation for metasomatic alteration. Econ Geol 81:1976–1982

Gunton CG (1999) A study of molybdenum at the Ernest Henry Cu–Au deposit, Northwest Queensland. BSc (Hons) thesis, unpublished. Australian National University

Gunton CG, Mavrogenes J, Blevin P (2000) Determination of fluid origins from trace element analysis of molybdenite at Ernest Henry, NW Queensland. In: Skilbeck CG, Hubble TCT (eds) Understanding Planet Earth: Searching for a sustainable future. Australian Geological Society, Abstract Series, 59:197

Haynes DW, Cross KC, Bills RT, Reed MH (1995) Olympic Dam ore genesis. A fluid mixing model. Econ Geol 90:281–307

Hemley JJ, Cygan GL, Fein JB, Robinson GR, D'Angelo WM (1992) Hydrothermal ore-forming processes in the light of studies in rock buffered systems: 1. iron-copper-zinc-lead sulphide solubility relations. Econ Geol 87:1–22

Hildebrand RS (1986) Kiruna-type deposits: their origin and relationship to intermediate subvolcanic plutons in the Great Bear Magmatic Zone, northwestern Canada. Econ Geol 81:640–659

Hitzman MW (2000) Iron oxide–Cu–Au deposits. What, where, when and Why. In: Porter TM (ed) Hydrothermal Iron Oxide Copper-Gold and Related Deposits: A Global Perspective. AMF, Adelaide, pp 9–26

Hitzman MW, Oreskes N, Einaudi MT (1992) Geological characteristics and tectonic setting of Proterozoic iron oxide (Cu–U–Au–REE) deposits. Precambrian Res 58:241–287

de Jong G, Williams PJ (1995) Giant metasomatic system formed during exhumation of mid-crustal Proterozoic rocks in the vicinity of the Cloncurry Fault, northwest Queensland. Aust J Earth Sci 42:281–290

Kodera P, Rankin AH, Lexa J (1998) Evolution of fluids responsible for iron skarn mineralization: an example from the Vyhne-Klokoc deposit, Western Carpathian, Slovakia. Min Pet 64:119–147

Kretz R (1983) Symbols for rock-forming minerals. Am Mineral 68:277–279

Lang JR, Stanley CR, Thompson JFH, Dunne KPE (1995) Na–K–Ca magmatic-hydrothermal alteration in alkalic porphyry Cu–Au deposits, British Columbia. In: Thompson JFH (ed) Magmas, fluids and ore deposits. Min Ass Canada Short Course Series 2, pp 339–366

Lindblom S, Broman C, Matinsson O (1996) Magmatic-hydrothermal fluids in the Pahtohavare Lentz DR, Walker JA, Stirling JAR (1995) Millstream Cu–Fe skarn deposit- an example of Cu-bearing magnetite-rich skarn system in northern New Brunswick. Explor Min Geol 4:15–31

Mark G (1998) Albitite formation by selective pervasive sodic-alteration of tonalite plutons in the Cloncurry district, NW Queensland. Australian J Earth Sci 45:765–774

Mark G, Foster DRW (2000) Magmatic albite-actinolite-apatite-rich rocks from the Cloncurry district, Northwest Queensland, Australia. Lithos 51:223–245

Mark G, Oliver NHS, Williams PJ, Valenta RK, Crookes RA (2000) The evolution of the Ernest Henry hydrothermal system. In: Porter TM (ed) Hydrothermal Iron Oxide Copper-Gold and Related Deposits. A Global Perspective. AMF, pp 123–136

Mark G, Foster DRW, Pollard PJ, Williams PJ, Tolman J, Darvall M (2004a) Magmatic fluid input during large-scale Na–Ca alteration in the Cloncurry Fe oxide–Cu–Au district, NW Queensland, Australia. Terra Nova 16:54–61

Mark G, Williams PJ, Boyce AJ (2004b) Low-latitude meteoric fluid flow along the Cloncurry Fault, Cloncurry District, NW Queensland, Australia: geodynamic and metallogenic implications. Chem Geol 207:133–148

Mark G, Stein HJ, Salt CJ (2004c) Re–Os isotopic evidence for periods of sulfide mineralization in the vicinity of the Ernest Henry Cu–Au deposit, Northwest Queensland, Australia. Geological Society of Australia, Abstracts 73, p 96

Mark G, Williams PJ, Ryan C, van Achterberg E, Prince K (2004d) A coupled microanalytical approach to resolving the origin of fluids and the genesis of ore formation in hydrothermal deposits. Geological Society of Australia, Abstracts 73, p 97

Mark G, Wilde A, Oliver NHS, Williams PJ (2005) Geochemical modelling of outflow from the Ernest Henry Fe oxide Cu–Au deposit: implication for ore genesis and exploration. J Geochem Explor 85:31–46

Marschik R, Fontboté L (2001) The Candelaria-Punta del Cobre Iron Oxide Cu–Au (–Zn–Ag) deposits, Chile. Econ Geol 96:1799–1826

Marshall LJ (2003) Brecciation within the Mary Kathleen Group of the Eastern Succession, Mount Isa block, Australia: implications for Fe-oxide-Cu-Au mineralization. Unpublished PhD Thesis, James Cook University of North Queensland, 325 pp

Marshall LJ, Oliver NHS (2005) Monitoring fluid chemistry in iron oxide–copper–gold-related metasomatic processes, eastern Mt Isa Block, Australia. Geofluids 5:1–22

Martinsson O, Wainhainen C (2000) Excursion Guide. In: Weihed P, Martinsson O (eds) Abstract volume and field guide workshop 2nd annual GEODE-Fennoscandian shield field workshop on Palaeoproterozoic and Archaean greenstone belts and VMS districts in the Fennoscandian Shield, Sweden. Luleå University of Technology, Report 6:63–76

Mathur R, Marschik R, Ruiz J, Munizaga F, Leveille, RA, Martin W (2002) Age of mineralization of the Candelaria iron oxide Cu–Au deposit, and the origin of the Chilean Iron Belt based on Re–Os isotopes. Econ Geol 97:59–71

McPhail DC (1993) The behavior of iron in high temperature chloride brines. Geological Society of Australia Abstracts Series 34:50–51

Menard J-J (1995) Relationship between altered pyroxene diorite and the magnetite mineralization in the Chilean Iron Belt, with emphasis on the El Algarrobo iron deposits (Atacama region, Chile). Miner Deposita 30:268–274

Oliver NHS, Valenta RK, Wall VJ (1990) The effect of heterogeneous stress and strain on metamorphic fluid flow, Mary Kathleen, Australia, and a model for large-scale fluid circulation. J Metamorphic Geol 8:311–331

Oliver NHS, Cartwright I, Wall VJ, Golding SD (1993) The stable isotope signature of kilometre-scale fracture-dominated metamorphic fluid pathways, Mary Kathleen, Australia. Metamorphic Geol 11:705–720

Oliver NHS, Cleverley JS, Mark G, Pollard PJ, Fu B, Marshall LJ, Rubenach MJ, Williams PJ, Baker T (2004) The role of sodic alteration in the genesis of iron oxide-copper-gold deposits, eastern Mt Isa Block, Australia. Econ Geol 99:1145–1176

Oreskes N, Einaudi MT (1992) Origin of hydrothermal fluids at Olympic Dam: preliminary results from fluid inclusions and stable isotopes. Econ Geol 87:64–90

Orville PM (1963) Alkali ion exchange between vapor and feldspar phases. Am J Sci 261:201–237

Page RW (1983) Chronology of magmatism, skarn formation and uranium mineralization, Mary Kathleen, Queensland, Australia. Econ Geol 78:838–853

Page RW (1988) Geochronology of early to middle Proterozoic fold belts in northern Australia: a review. Precam Res 40–41:1–19

Page RW (1998) Links between Eastern and Western fold belts in the Mount Isa Inlier, based on SHRIMP U–Pb studies. Geological Society of Australia Abstracts 49:349

Page RW, Sun S-S (1998) Aspects of geochronology and crustal evolution in the Eastern Fold Belt, Mount Isa Inlier. Aust J Earth Sci 45:343–362

Page RW, Sweet IP (1998) Geochronology of basin phases in the western Mount Isa Inlier, and correlation with the McArthur Basin. Aust J Earth Sci 45:219–232

Pearson PJ, Holcombe RJ, Page RW (1992) Synkinematic emplacement of the middle Proterozoic Wonga Batholith into a midcrustal extensional shear zone, Mt Isa Inlier, Queensland, Australia. In: Stewart AJ, Blake DH (eds) Detailed studies of the Mount Isa Inlier. Australian Geological Survey Organization Bulletin 243:289–328

Perkins C, Wyborn L (1998) Age of Cu–Au mineralization, Cloncurry district, Mount Isa Inlier, as determined by $^{40}Ar/^{39}Ar$ dating. Aust J Earth Sci 45:233–246

Perring CS, Pollard PJ, Dong G, Nunn AJ, Blake KL (2000) The Lightning creek sill complex, Cloncurry district, northwest Queensland: A source of fluids for Fe oxide Cu–Au mineralisation and sodic-calcic alteration. Econ Geol 95:1067–1089

Pidgeon RT, Bosch D, Bruguier O (1996) Inherited zircon and titanite U–Pb systems in an Archaean syenite from southwestern Australia: Implications for U–Pb stability of titanite. Earth Planet Sc Lett 141:187–198

Pollard PJ (2000) Evidence of a magmatic fluid and metal source for Fe-oxide Cu–Au mineralization. In: Porter TM (ed) Hydrothermal Iron Oxide Copper-Gold and Related Deposits: A Global Perspective. AMF 1:27–41

Pollard PJ (2001) Sodic(-calcic) alteration in Fe oxide–Cu–Au districts: an origin via unmixing of magmatic H_2O–CO_2–$NaCl \pm CaCl_2$–KCl fluids. Miner Deposita 36:93–100

Pollard PJ, McNaughton N (1997) U–Pb geochronology and Sm/Nd isotope characteristics of Proterozoic intrusive rocks in the Cloncurry district, Mount Isa Inlier, Australia. In: Pollard, PJ (compiler) AMIRA P438 Final Report: Cloncurry Base Metals and Gold Section 4, p 19

Pollard PJ, Perkins C (1997) $^{40}Ar/^{39}Ar$ geochronology of alteration and Cu–Au–Co mineralization in the Cloncurry district, Mount Isa Inlier, Australia. In: Pollard PJ (compiler) AMIRA P438 Final Report: Cloncurry Base Metals and Gold Section 3, p 40

Pollard PJ, Mark G, Mitchell LC (1998) Geochemistry of post-1540 granites spatially associated within regional sodic-calcic alteration and Cu–Au–Co mineralization, Cloncurry district, northwest Queensland. Econ Geol 93:1330–1344

Proffett JM (2003) Geology of the Bajo de la Alumbrera porphyry copper-gold deposit, Argentina. Econ Geol 98:1535–1574

Rankin AH, Ramsey MH, Coles B, Vanglangvelde F, Thomas CR (1992) The composition of hypersaline iron-rich granitic fluids based on laser-ICP and synchrotron XRF microprobe analysis of individual inclusions in topaz, Mole Granite, eastern Australia. Geochim Cosmochim Acta 56:67–79

Requia K, Stein H, Fontboté L, Chiaradia M (2003) Re–Os and Pb–Pb geochronology of the Archean Salobo iron oxide copper–gold deposit, Caraja's mineral province, northern Brazil. Miner Deposita 38:727–738

Richardson CK, Holland HD (1979) Fluorite deposition in hydrothermal systems. Geochim Cosmochim Acta 43:1327–1335

Rotherham JF, Blake KL, Cartwright I, Williams PJ (1998) Stable isotope evidence for the origin of the Starra Au–Cu deposit, Cloncurry district. Econ Geol 93:1435–1449

Rubenach MJ, Lewthwaite KA (2002) Metasomatic albitites and related biotite-rich schists from a low-pressure polymetamorphic terrane, Snake Creek Anticline, Mount Isa Inlier, northeastern Australia. microstructures and P-T-d paths. J Metam Geol 20:191–202

Rubenach MJ, Adshead ND, Oliver NHS, Tullemans F, Esser D, Stein H (2001) The Osborne Cu–Au deposit: geochronology, and genesis of mineralization in relation to host albitites and ironstones. In: Williams PJ (ed) 2001: a hydrothermal odyssey, new developments in metalliferous hydrothermal systems research, extended conference abstracts. JCU EGRU Contrib 59:172–173

Ryan A (1998) Ernest Henry copper-gold deposit. In: Berkman DA, Mackenzie DH (eds) Geology of Australian and Papua New Guinean Mineral Deposits. Australasian Inst Mining Metall 22:759–768

Seedorf E, Einaudi MT (2004) Henderson porphyry molybdenum system, Colorado: II. Decoupling of introduction and deposition of metals during geochemical evolution of hydrothermal fluids. Econ Geol 99:39–72

Sillitoe RH (2003) Iron oxide-copper-gold deposits: an Andean view. Miner Deposita 38:787–812

Skirrow RG (2000) Gold–Copper–Bismuth deposits of the Tennant Creek District, Australia: a reappraisal of diverse high-grade systems. In: Porter TM (ed) Hydrothermal iron oxide copper–gold and related deposits: a global perspective. AMF, pp 149–160

Skirrow RG, Walshe JL (2002) Reduced and oxidized Au–Cu–Bi iron oxide deposits of the Tennant Creek Inlier, Australia. An integrated geological and chemical model. Econ Geol 97:1167–1202

Sverjensky DA, Hemley JJ, D'Angelo WM (1991) Thermodynamic assessment of hydrothermal alkali feldspar-mica-aluminosilicate equilbria. Geochem Cosmochim Acta 55:989–1004

Twyerould SC (1997) The geology and genesis of the Ernest Henry Fe–Cu–Au deposit, northwest Queensland, Australia. PhD thesis, unpublished. University of Oregon

Ulrich T, Günthur D, Heinrich CA (2001) The evolution of a porphyry Cu–Au deposit, based on LA-ICP-MS analysis of fluid inclusions: Bajo de la Alumbrera. Argentina Econ Geol 96:1743–1774

Vidal CE (1986) Metallogenesis associated with the Coastal Batholith of Peru: a review. In: Pitcher WS et al (eds) Magmatism at a plate edge: the Peruvian Andes. Blackie, Glasgow, pp 243–249

Wang S, Williams PJ (2001) Geochemistry and origin of Proterozoic skarns at the Mount Elliott Cu–Au (–Co–Ni) deposit, Cloncurry district, NW Queensland. Miner Deposita 36:109–124

Wanhainen C, Broman C, Martinsson O (2003) The Aitik Cu–Au–Ag deposit in northern Sweden: a product of high salinity fluids. Min Dep 38:715–726

Webb M, Rowston P (1995) The geophysics of the Ernest Henry Cu–Au deposit (N.W.) Queensland. Expl Geophys 26:51–59

Williams PJ (1994) Iron mobility during synmetamorphic alteration in the Selwyn Range area, NW Queensland: Implications for the origin of ironstone-hosted Au–Cu deposits. Miner Deposita 29:250–260

Williams PJ (1998) Metalliferous economic geology of the Mount Isa Eastern Succession, Queensland. Australian J Earth Sci 45:329–342

Williams PJ, Heineman M (1993) Maramungee: a Proterozoic Zn skarn in the Cloncurry district, Mt Isa Inlier, Queensland, Australia. Econ Geol 88:1114–1134

Williams PJ, Pollard PJ (2003) Australian Proterozoic iron oxide–Cu–Au deposits: an overview with new metallogenic and exploration data from the Cloncurry district, northwest Queensland. Explor Mining Geol 10:191–213

Williams PJ, Skirrow RG (2000) Overview of Iron Oxide-Copper-Gold deposits in the Curnamona Province and Cloncurry district (Eastern Mount Isa Block), Australia. In: Porter TM (ed) Hydrothermal Iron Oxide Copper-Gold and Related Deposits: A Global Perspective. AMF, pp 105–122

Williams PJ, Dong G, Ryan CG, Pollard PJ, Rotherham J, Mernagh TP, Chapman LH (2001) Geochemistry of hypersaline fluid inclusions from the Starra (Fe oxide)–Cu–Au deposit, Cloncurry district, Queensland. Econ Geol 96:875–884

Wyborn LAI, Page RW, McCulloch MT (1988) Petrology, geochronology and isotope geochemistry of the post-1820 Ma granites of the Mount Isa Inlier: mechanisms for the generation of Proterozoic anorogenic granites. Precam Res 40–41:509–541